

FACULTY OF CHEMISTRY DEPARTMENT OF PHYSICAL CHEMISTRY AND TECHNOLOGY OF POLYMERS

Organic monolayers-based protective coatings for bioelectronic devices Organiczne monowarstwy jako powłoki ochronne w urządzeniach bioelektronicznych

mgr. Taral Patel

Supervisor: dr hab. inż. Katarzyna Krukiewicz, prof. PŚ

Table of contents

Abstract5
Streszczenie
List of publications
Nomenclature
1. Introduction
2. Hypothesis and research objectives
3. Methodology
3.1. Literature studies
3.2. Electrode preparation and surface modification
3.3. Functional coating strategies
3.4. Electrochemical characterization
3.5. Physicochemical characterization
3.6. Stability testing
3.7. Biological characterization
4. Results and discussion
4.1 Surface modification strategies for tunable cell adhesion and neural interface biointegration
4.1.1. Affecting cell adhesion through surface functionalization
4.1.2. Advancing neural selectivity through poly-L-lysine/laminin co-immobilization
4.2. Enhancing PEDOT:PSS adhesion and charge transfer by surface modification30
4.3. Mixed thiol self-assembled monolayers for neural interface engineering40
5. Summary
6. Literature
Summary of personal contribution
List of scientific accomplishments
Appendix62

Abstract

Implantable bioelectronic devices promise precise diagnosis and therapy, yet their durability is often decided at the interface where metal meets living tissue. Mechanical mismatch, and nonspecific biofouling trigger glial activation and fibrotic encapsulation that compromise device's performance. Coating the surface of the metals with organic layers can serve as a promising strategy to improve the biocompatibility of bioelectronic devices. Nevertheless, even when device performance is improved in the short term, many coatings struggle with poor long-term adhesion and limited chemical control of cell interactions, all of which constrain reliable, chronic operation.

This thesis responds to the current needs in biomedical sector by introducing ultrathin, covalently anchored organic layers that are molecularly programmed to couple electrical stability with biological selectivity. Pro-adhesive ligands have been used to develop neuron-preferring surfaces that enhance neural adhesion and differentiation while tempering astrocytic responses. Adhesion-promoting interlayers have been used to stabilize conducting polymer films without compromising their conductive and capacitive behavior. Composition-tuned mixed monolayers have been introduced as a way to provide fine control of wettability and interfacial charge, supporting neurite outgrowth while limiting astrocytic branching. Together, these outcomes yield clear structure-function design rules and a modular, scalable strategy for building reliable, long-lived, and multifunctional bioelectronic interfaces advancing the practical engineering of next-generation neural electrodes and implantable biosensors.

Streszczenie

Wszczepialne urządzenia bioelektroniczne mogą zrewolucjonizować diagnostykę i terapię wielu chorób, lecz o ich trwałości wciąż przesądzają zjawiska występujące na granicy kontaktu metalu z żywą tkanką. Niedopasowanie mechaniczne oraz nieselektywne pokrycie powierzchni biocząsteczkami i komórkami powoduje aktywację komórek glejowych i powstawanie blizny glejowej, a w konsekwencji zmniejszenie wydajności urządzenia. Pokrycie powierzchni metalu warstwą organiczną uważane jest za skuteczny sposób na zwiększenie biokompatybilności urządzeń biomedycznych. Niemniej jednak, poprawa jest zwykle krótkotrwałą, wiele powłok bowiem nie wykazuje wystarczająco dobrej adhezji do podłoża, w ograniczony sposób oddziałuje z komórkami organizmu, co ogranicza długotrwałą skuteczność działania urządzenia.

Niniejsza praca odpowiada na te wyzwania poprzez wprowadzenie ultracienkich, kowalencyjnie unieruchomionych warstw organicznych, programowanych molekularnie tak, aby łączyły stabilność elektryczną z selektywnością biologiczną. Wykorzystanie związków proadhezyjnych umożliwiło uzyskanie powierzchni preferujących interakcje z neuronami, które wzmacniają ich adhezję i różnicowanie, a jednocześnie łagodzą odpowiedź astrocytów. Właściwości proadhezyjne powłok wpłynęły również na poprawę stabilności osadzonych warstw polimerów przewodzących, zachowując ich wysokie przewodnictwo elektryczne i pojemność elektryczną. Mieszane monowarstwy o regulowanym składzie zapewniły precyzyjną kontrolę zwilżalności i ładunku międzyfazowego, promując wzrost neurytów przy równoczesnym ograniczeniu rozgałęziania astrocytów. Wyniki te pozwalają na opracowanie jasnych zasad projektowania powłok biomedycznych oraz modułowej, skalowalnej strategii tworzenia trwałych i wielofunkcyjnych interfejsów bioelektronicznych, które przyczyniają się do rozwoju praktycznej inżynierii elektrod neuronowych i wszczepialnych biosensorów nowej generacji.

List of publications

The presented doctoral thesis is based on the following publications:

[R1] T. Patel, J. Huang, K. Krukiewicz, Multifunctional organic monolayer-based coatings for implantable biosensors and bioelectronic devices: Review and perspectives, *Biosensors and Bioelectronics: X*, 14, 100349 (2023). https://doi.org/10.1016/j.biosx.2023.100349
MNiSW = 20

[R2] T. Patel, M. Skorupa, M. Skonieczna, R. Turczyn, K. Krukiewicz, Surface grafting of poly-L-lysine via diazonium chemistry to enhance cell adhesion to biomedical electrodes, *Bioelectrochemistry*, 152, 108465 (2023). https://doi.org/10.1016/j.bioelechem.2023.108465 MNiSW = 100; IF = 4.5.

[R3] T. Patel, M. Skonieczna, R. Turczyn, K. Krukiewicz, Modulating pro-adhesive nature of metallic surfaces through a polypeptide coupling via diazonium chemistry, *Scientific Reports*, 13, 18365 (2023). https://doi.org/10.1038/s41598-023-45694-z MNiSW = 140; IF = 3.9.

[R4] S. Smołka*, T. Patel*, S. Pluczyk-Małek, R. Turczyn, K. Krukiewicz, Iodonium-based pro-adhesive layers for robust adhesion of PEDOT:PSS to surfaces, *Science and Technology of Advanced Materials*, 25(1), 2338786 (2024). https://doi.org/10.1080/14686996.2024.2338786 MNiSW = 100; IF = 6.9 (*equal contribution).

[R5] T. Patel, M. Sankar, K. Krukiewicz, M. Biggs, Engineering gold biointerfaces with mixed short-chain thiols: electrochemical and cellular studies, *Colloids and Surfaces B: Biointerfaces*, 115230 (2025). https://doi.org/10.1016/j.colsurfb.2025.115230
MNiSW = 100; IF = 5.6

Nomenclature

AB Aminobenzene

AB/PL/EDC AB layer with poly-L-lysine covalently immobilized via EDC coupling AB/PL/LM/EDC AB layer with covalently co-immobilized poly-L-lysine and laminin via

EDC coupling

AC Alternating current

ACN Acetonitrile

AFM Atomic force microscopy

Ag/AgCl Silver/silver-chloride reference electrode

ATR Attenuated total reflectance

B-27 neuronal culture supplement

CPE Constant-phase element
CSC Charge storage capacity

CTR Tissue-culture plastic control sample

CV Cyclic voltammetry

DCM Dichloromethane

DMEM/F12 Dulbecco's Modified Eagle Medium/Nutrient Mixture F-12

EDC 1-Ethyl-3-(3-dimethylaminopropyl)carbodiimide

EIS Electrochemical impedance spectroscopy

EMEM Eagle's Minimum Essential Medium

EQCM Electrochemical quartz crystal microbalance

EtOAc Ethyl Acetate

FBS Fetal bovine serum
FD Fractal dimension

FTIR Fourier-transform infrared spectroscopy

LM Laminin

ME 2-Mercaptoethanol

NB Nitrobenzene

PBS Phosphate-buffered saline

PEDOT Poly(3,4-ethylenedioxythiophene)

PEDOT:PSS Poly(3,4-ethylenedioxythiophene):poly(styrene sulfonate)

PL Poly-L-lysine

PSS Poly(styrene sulfonate)

R_{CT} Charge-transfer resistance

R_s Solution resistance

S_a Arithmetic mean height (areal surface roughness parameter)

SAM Self-assembled monolayer

Salt A Bis(4-tertbutylphenyl)iodonium hexafluorophosphate

Salt B (4-nitro-phenyl)(2,4,6-trimethylphenyl)iodonium triflate

Salt C Diphenyliodonium chloride

Salt D Bis(4-methylphenyl)iodonium hexafluorophosphate

SH-SY5Y Human neuroblastoma cell line

tBu₄NBF₄ Tetrabutylammonium tetrafluoroborate

tBu₄NPF₆ Tetrabutylammonium hexafluorophosphate

TT 2-Thiophenethiol

U87 Human glioblastoma-astrocytoma cell line

UV-Vis Ultraviolet-visible spectroscopy

1. Introduction

The development of implantable biosensors and neural interfaces has transformed modern medicine by enabling direct communication between electronic devices and the nervous system. These technologies underpin diagnostic platforms, neuromodulation therapies, and brain-computer interfaces, where electrodes serve as the critical points of contact with biological tissue¹. For long-term success, such devices must combine electrical efficiency with stable, defined interactions at the tissue-electrode interface². However, despite decades of progress, implant performance remains limited by biofouling, foreign body reaction, and mechanical and chemical instability at this delicate interface^{3–5}.

Noble metals such as platinum, gold, and iridium have long been the standard materials for electrodes due to their chemical stability and conductivity. However, the chemical and mechanical mismatch between the electrode surface and a living tissue is the factor that triggers foreign body reactions, including astrocyte activation and glial scar formation, which insulate electrodes and degrade signal quality. Furthermore, metallic surfaces are prone to nonspecific protein adsorption which compromise device longevity^{6,7}.

To address these challenges, various coating strategies have been explored. Conducting polymers, particularly PEDOT:PSS, reduce impedance and increase charge transfer while offering improved mechanical softness⁸. Nevertheless, their clinical translation is hindered by poor adhesion to metal substrates and delamination under electrical and physiological stress. Hydrogel coatings can encapsulate bioactive cues and better mimic tissue mechanics, but their swelling behavior and limited durability restrict their application⁹. Nanostructured carbons provide high surface area and excellent conductivity, yet their bioactivity is difficult to control, as they lack molecular-level programmability¹⁰.

As a result, there has been a growing interest in molecular coatings that offer precise chemical control at the electrode surface. Diazonium electrografting produces thin, covalently bound aryl films that resist desorption and can be further functionalized. Iodonium salts, another class of aryl donors, provide more reproducible grafting and can act as adhesion promoters for polymer films^{11,12}. Thiol-based self-assembled monolayers (SAMs) on gold allow systematic tuning of surface wettability, charge, and functional group presentation through controlled molecular composition¹³. These approaches have the potential to stabilize coatings, improve electrochemical performance, and induce direct cell-specific interactions. Yet, despite their

promise, challenges remain: diazonium films often form highly cross-linked layers that hinder controlled modification¹⁴; thiol-based SAMs can undergo oxidative degradation in biological media; and systematic correlations between molecular design, electrochemical properties, and biological outcomes remain underexplored¹⁵.

These limitations point to a critical need for strategies that integrate the robustness of covalent chemistry with the selectivity of molecular self-assembly vital requirement for long-term implants. This thesis responds to these needs by investigating ultrathin organic layers, prepared through electrografting of aryl salts and thiol self-assembly, as multifunctional coatings for implantable electrodes. The aim is not only to enhance electrochemical stability but also to fine-tune cellular compatibility thereby advancing the design of next generation biointerfaces.

2. Hypothesis and research objectives

In my research, I hypothesized that surface modification strategies based on ultrathin organic layers, formed either through the electrografting of onium salts, or self-assembly of thiols, can be rationally designed to improve cellular compatibility and electrochemical performance of metal-based electrodes used in bioelectronic applications. Accordingly, I formulated the following research objectives:

- 1. To conduct a comprehensive review of the existing literature in order to identify research gaps and highlight the most effective strategies for addressing them.
- 2. To fabricate stable, covalently anchored organic layers on conductive substrates (platinum and gold) via electrochemical reduction of aryl diazonium and iodonium salts, enabling further biofunctionalization and conductivity control.
- To investigate and compare strategies for immobilizing biologically active molecules, such as poly-L-lysine and laminin on diazonium-modified surfaces, using both physical and covalent coupling methods.
- 4. To improve the adhesion, electrochemical integrity, and mechanical stability of conducting polymer coatings by introducing iodonium-based adhesion-promoting interlayers and evaluate their impact on charge transfer resistance and capacitive behaviour.

- To develop and characterize mixed self-assembled monolayers of selected thiols on gold electrodes as a means to modulate surface hydrophilicity, nano-roughness, and electrochemical impedance.
- 6. To perform comprehensive surface characterization of modified electrodes including wettability, topography, and electrochemical impedance combined with biological evaluation using cell viability, and adhesion assays.

The research outcomes have been published in peer-reviewed international journals. This doctoral dissertation provides an overview of the key findings, with emphasis on the sections that reflect my direct contributions during the PhD.

3. Methodology

This chapter outlines the experimental methodologies employed across the five studies constituting the research foundation of this dissertation. The methods were grouped by functional objectives, from electrode preparation and chemical modification to physicochemical and biological characterization. Each subsection concludes with the relevant reference to the associated paper [R1–R5].

3.1 Literature studies

To ensure a comprehensive and up-to-date understanding of the field, the relevant publications were searched through different keywords bioelectronic devices, implantable biosensors, organic monolayers, self-assembled monolayers (SAMs), diazonium coatings, iodonium salts, sulfonium-based monolayers, electrografting, covalent surface functionalization, and surface modification techniques. To expand the search and capture studies on clinical relevance and device performance, additional terms included biocompatibility, biofouling, bacterial colonization, in vivo stability, corrosion resistance, tissue-electrode interface, functional coatings, neural electrodes, conducting polymers, thiol-gold chemistry, and flexible and biodegradable bioelectronics. Boolean operators (AND/OR) were applied to refine results, for example: electrografting AND biomedical electrodes or SAMs AND protein adsorption. Filters were applied to include only peer-reviewed articles, particularly from the past decade, to reflect recent developments. Preference was given to high-impact journals in bioelectronics, materials science, analytical chemistry, and biomedical engineering. Literature was obtained from multiple scientific databases: PubMed (http://www.ncbi.nlm.nih.gov/pubmed), Google Scholar (http://www.scholar.google.com), Elsevier (https://www.elsevier.com/en), Science Direct (http://www.sciencedirect.com), Wiley (http://www.onlinelibrary.wiley.com), Springer (http://www.springer.com), and Scopus (http://www.scopus.com) [R1].

3.2 Electrode preparation and surface modification

Platinum-coated and gold-coated Thermanox coverslips (NUNC, Rochester, NY, USA) were used as the primary substrates. Platinum sputter-coating was performed using a Q150R rotary-pump sputter coater (Quorum Technologies, UK), resulting in 78–84 nm thick metallic layers with a conductivity of 4.3×10^5 S m⁻¹. Gold sputtering process was done using Emitech K650Xt sputter coater with the operating parameters of 25 mA, 1×10^{-3} mbar and time 210 s [R2, R3, R4, R5]. Prior to use, substrates were cleaned with deionized water and dried under air.

Electrografting of aryldiazonium salts was performed by preparing 3 mM solutions of the selected aryldiazonium salt (4-nitrobenzenediazonium (DAZ 1), 4-methoxybenzenediazonium (DAZ 2), and 3,5-dichlorophenyldiazonium (DAZ 3)), in 0.1 M tetrabutylammonium tetrafluoroborate/acetonitrile (*t*Bu₄NBF₄/ACN) solution. The electrochemical grafting was conducted in a three-electrode configuration using a CHI 660C potentiostat (CH Instruments, USA), or PalmSens4 (PalmSens, Netherlands) with a platinum wire as the counter electrode, Ag/AgCl (3M KCl) as the reference electrode, and coated Thermanox coverslips as the working electrode through cyclic voltammetry by applying potential between -0.9 V and +0.5 V (vs. Ag/AgCl) for 5 CV cycles at a scan rate of 50 mV s⁻¹ [R2, R3]. Reduction of 4-nitrobenzenediazonium salt (DAZ 1) to 4-aminobenzenediazonium salt (DAZ 4) was done in the above mentioned three electrode setup in 0.1 M KCl/water:ethanol (9:1 v/v). Cyclic voltammograms were collected from 0.2 V to 1.0 V for 5 CV cycles with a scan rate of 50 mV s⁻¹ [R2, R3].

For the electrografting of diaryliodonium salts, four iodonium derivatives were used: iodonium hexafluorophosphate (Salt A), (4-nitrophenyl)(2,4,6-trimethylphenyl)iodonium triflate (Salt B), diphenyliodonium chloride (Salt C) and bis(4-methylphenyl)iodonium hexafluorophosphate (Salt D) [R4]. Three salts (Salt A, Salt B, Salt D) were dissolved in acetonitrile (3 mM of salt in 0.1 M tBu₄NPF₆/ACN), while diphenyliodonium chloride (Salt C) was dissolved in water containing 0.1 M KNO₃ as a supporting electrolyte. CV was performed for specific potentials for individual salts at 50 mV s⁻¹ under ambient conditions using the same electrochemical setup as described previously.

3.3 Functional coating strategies

Diazonium coated Pt surfaces were coated with Poly-L-lysine (PL) and Laminin (LM) via drop-casting PL solution (0.1% w/v, 20 μl - 40 μl) or PL/LM solution (0.1% w/v, 40 μl) on diazonium-modified surfaces. In EDC (1-ethyl-3-(3-dimethylaminopropyl)carbodiimide) coupling method, the electrodes were submerged into a solution containing 6 mM EDC in a phosphate buffered saline (PBS) (one tablet providing a buffer solution containing 0.01 M phosphate buffer, 0.0027 M potassium chloride, 0.137 M sodium chloride when dissolved in 200 ml ultrapure water) in 30 μl of either PL or PL/LM solution [R2, R3]. After 1 hour of incubation at room temperature, the electrodes were rinsed and air-dried. Poly(3,4-ethylenedioxythiophene):poly(styrene sulfonate) (PEDOT:PSS) films were applied onto

iodonium-modified Pt surfaces by drop-casting 200 µl 1.1% PEDOT:PSS water dispersion followed by drying at 60°C for 30 min [R4].

Thiol-based self-assembled monolayers (SAMs) were prepared by immersing gold-coated Thermanox coverslips in binary mixture solutions of 2-thiophenethiol (TT) and 2-mercaptoethanol (ME) with different composition as shown in Table 1. After 24 hours, surfaces were rinsed thoroughly with deionized water and air dried [R5].

Sample name	1:0	1:0.5	1:1	0.5:1	0:1
TT volume, ml	3	2	1.5	1	0
ME volume, ml	0	1	1.5	2	3

Table 1. Encoding of investigated samples.

3.4 Electrochemical characterization

Electrochemical characterization was carried out using cyclic voltammetry (CV) and electrochemical impedance spectroscopy (EIS). CV was used to monitor the electrodeposition process and determine redox features, while EIS was employed to assess surface impedance and capacitive behaviour across 0.1~Hz-100kHz frequency range, at a DC potential of 0~V to 0.2~V with an AC amplitude of 50-100~mV in PBS solution [R2, R3, R4, R5]. The impedance spectra were fitted to equivalent circuit models using the EIS Spectrum Analyzer software 16 . The optimization was performed with Nelder-Mead simplex (NM simp) or Powell algorithms, which minimized the χ^2 error between experimental and simulated spectra, enabling extraction of parameters such as R_S , R_{CT} , and capacitance.

The electrochemical studies were performed by means of a potentiostat equipped with a three-electrode system mentioned earlier. Cyclic voltammograms were collected with a scan rate of 100 mV s⁻¹ in 0.1 M of a corresponding electrolyte. Charge storage capacity (CSC, mC cm⁻²) was calculated with the use of the following equation:

$$CSC = \frac{1}{A \cdot v} \int_{V_1}^{V_2} I(V) \, dV$$

where: A is electrode area (0.283 cm²), v is a scan rate (V s⁻¹), V is the potential (V) and I is current (A). V_1 and V_2 represent the potential range of a single scan.

Capacitance (C, F) of a constant phase element, which works as a pseudo capacitor in the EIS circuit [R3], was calculated by the following equation:

$$C = \frac{(Q \cdot R_{CT})^{\left(\frac{1}{n}\right)}}{R_{CT}}$$

where Q is the CPE parameter, R_{CT} is the charge transfer resistance (Ω) and n is the CPE exponential parameter.

Electrogravimetric investigations were performed via a time resolved electrochemical quartz crystal microbalance (EQCM, CHI 400C, CH Instruments, Texas, U.S.A) using CHI 125 gold crystal electrodes. Mass change was correlated with frequency change by the following equation:

$$\Delta f = -\frac{2f_0^2}{A\sqrt{\rho_q \mu_q}} \Delta m$$

where: ρ_q means a density of quartz (2.648 g cm⁻³), μ_q is a shear modulus of quartz (2.947·10¹¹ g cm⁻¹ s⁻²), A is an electrode surface (0.205 cm²), f_0 is a resonant frequency of the fundamental mode (Hz), Δ m is a mass change (g). For $f_0 = 7.995$ MHz, the mass change correlated to a frequency change of 1 Hz is equal to 1.4 ng [R2, R4].

3.5 Physicochemical characterization

Surface morphology was characterized using optical profilometer (Filmetrics Profilm 3D, CA, U.S.A) by arithmetic mean height (S_a) parameter according to ISO 25178 [R2, R3] and atomic force microscopy (AFM), and particularly CoreAFM Nanosurf, Switzerland with the application of a phase contrast (tapping mode) using Tapping Mode HQ:NSC15/AIBS AFM Probe (MikroMasch, CA, U.S.A.) [R4], Dimension 3100 AFM operated by NanoScope IIIa controller in a tapping mode with the use of a TESPA silicon probe (tip height 10–15 μm, tip radius cantilever force constant of 42 Nm⁻¹) [R5]. Surface roughness (S_a) values were calculated from 3D images using ImageJ software [R4, R5]. Wettability of the surface coatings was analysed by goniometry performed at 20 °C via an optical goniometer (OCA15 Dataphysics) by suspending 1 μl drop ultrapure water droplets on the investigated surfaces [R2, R3, R4, R5]. FTIR spectroscopy (PerkinElmer Spectrum Two IR spectrometer) was conducted using ATR mode with a spectral range between 500-4000 cm⁻¹ and resolution of 2 cm⁻¹ to confirm surface chemistry [R2, R3]. Additionally, Raman spectroscopy (Renishaw InVia,

Renishaw, Wotton under Edge, UK) was used to identify molecular features of aryl and peptide coatings [R2, R3, R4].

3.6 Stability testing

To assess the impact of iodonium treatment on PEDOT:PSS adhesion, modified electrodes were immersed in 2 ml of PBS and stored in sealed containers for 30 days in the dark to minimize evaporation. After ageing, the PBS solutions were analysed via UV-Vis spectroscopy (HP 8453, Hewlett Packard), and cyclic voltammetry was performed before and after ageing to determine CSC [R4]. To evaluate adhesion strength of PEDOT:PSS films, tape peel test was conducted by covering the PEDOT:PSS modified surfaces with a tape, which was removed after 30 s, maintaining 90° angle for each sample [R4].

3.7 Biological characterization

Cell-based evaluation was performed using either SH-SY5Y neuroblastoma cell lines [R2, R3], U87 derived from glioblastoma cells [R3] or primary mesencephalic cultures from rat embryos [R5]. SH-SY5Y cells were seeded at 5×10⁴ cells per cm² on modified electrodes and cultured in DMEM/F12 with 10% FBS and 1% penicillin/streptomycin at 37 °C in 5% CO₂. U87 were seeded at 5×10^4 cells per cm² on modified electrodes and cultured in EMEM with 10% FBS and 1% penicillin/streptomycin at 37 °C in 5% CO₂. Primary mesencephalic cultures from the ventral mesencephalon of rat embryos were dissected from embryonic 14 day rat brains and then mechanically dissociated with a pipette, until the tissue was dispersed. Cells were grown in a humidified atmosphere of 5% CO₂ at 37 °C and cultured in medium (DMEM/F12, 0.033 M D-glucose, 1% L-glutamine, 1% penicillin/streptomycin, 1% fetal calf serum, supplemented with 2% B27). After incubation, cell morphology and coverage were assessed by confocal microscopy and automated cell imaging systems (JuLITM FL, NanoEnTek) [R2,R3]. For primary cultures, astrocytes and neurons were differentially labelled immunofluorescence and visualized using confocal microscopy. Fractal dimension analysis was performed on neurons and astrocytes using ImageJ and fractal box count method [R5].

4. Results and discussion

4.1 Surface modification strategies for tunable cell adhesion and neural interface biointegration

4.1.1 Affecting cell adhesion through surface functionalization

Aryl diazonium salts have emerged as powerful tools for tailoring surface chemistry of conductive materials through electrografting, forming covalently anchored, stable, and tuneable organic interlayers¹⁷. Prior studies have explored diazonium-functionalized surfaces for applications such as corrosion resistance, biosensing, and electrochemical tuning ^{18,19}. For instance, poly(ethylene terephthalate) (PET) surfaces that were functionalized with diazonium salts provided a stable platform for covalent grafting of bioactive layers. Coatings such as poly(2-hydroxyethyl methacrylate) and fibronectin could be firmly anchored to the modified surface of PET, resulting in surfaces that not only supported biosensing functions but also improved cell adhesion and facilitated muscle cell differentiation.²⁰. Separately, poly-L-lysine (PL) is widely used as a pro-adhesive agent to promote neuronal cell adhesion due to its positively charged amine groups, which interact favourably with negatively charged cell membranes²¹. So far, PL has been extensively studied for enhancing neural cell adhesion, though typically via simple physisorption or adsorption onto oxide or polymer surfaces^{22,23}. However, there is a marked gap in the literature where these two strategies are integrated, specifically the use of electrografted diazonium monolayers as covalent anchoring platforms for PL in neural electrode interfaces. This interface design could offer not only improved neural adhesion and long-term coating stability, but also a platform to investigate how surface-bound PL affects both electrochemical and biological performance.

To address this, I employed three diazonium salts with distinct electronic characteristics 4-nitrobenzenediazonium (DAZ 1), 4-methoxybenzenediazonium (DAZ 2), and 3,5-dichlorophenyldiazonium (DAZ 3) chosen to represent electron-withdrawing (NO₂, Cl) and electron-donating (OCH₃) substituents, enabling a comparative analysis of how the choice of substituent influences electrochemical behaviour and cell–surface interactions on platinum electrodes. Among the three salts, DAZ 1 could be further reduced to 4-aminobenzene (DAZ 4) by cyclic voltammetry. The electrodeposition of aryl diazonium salts was performed to create robust, covalently anchored organic layers on platinum substrates intended for biointerface applications [R2]. These processes were monitored using CV and EQCM, which revealed deposition rates differing among the tested diazonium species.

Using potentiodynamic electroreduction in an acetonitrile-based electrolyte, I observed irreversible cathodic peaks characteristic of diazonium reduction, confirming the generation of aryl radicals and their subsequent grafting onto the metal surface (Figure 1 (A, B, C)). Corresponding CV curves show a broad, irreversible cathodic peak observed during the first scan, which is characteristic of diazonium salt reduction via one-electron transfer process. The disappearance of the cathodic peak in subsequent cycles indicates rapid passivation of the surface due to formation of a compact organic layer that blocks further electron transfer. DAZ 1 and DAZ 3 show complete peak attenuation by the third scan, reflecting high surface reactivity and fast saturation shown in Figure 1 (A) and (C). In contrast, CV of DAZ 2 shows the reduction occurring slower with subsequent cycles that in turn reflects to lesser surface coverage which was supported by EQCM results.

Among the three electroreduced diazonium-derived moieties, DAZ 1 could be further reduced to 4-aminobenzene. The reduction of nitro group to amino group and forming DAZ 4 was performed in 0.1 M KCl/water:ethanol (9:1 v/v). A CV curve was collected from the potential of 0.2 V to -1.0 V (vs. Ag/AgCl) for 5 CV cycles demonstrating the reduction process occurring on the surface of the electrode (Figure 1(D). Reduction of 4-nitrobenzene proceeds via two main steps: firstly, a reduction of 4-nitrobenzene to 4-phenylhydroxylamine (PHA) takes place through a four-electron exchange, forming 4-nitrosobenzene (NSB) intermediate. Following, the PHA converts to 4-aminobenzene via a two-electron reduction process. NHB remains undetected due to its rapid conversion to PHA, and unstable PHA swiftly converts to 4-aminobenzene²⁴.

Electrode coated with DAZ 1 derivative exhibited the highest mass gain $(203.63 \pm 5.69 \text{ ng})$ and rapid film formation (within 260 sec), indicating efficient reduction and grafting under the applied conditions. Although the highest currents were noted during the deposition of DAZ 2, it was DAZ 1 that resulted in the formation of the heaviest deposit. It could be partially derived from the difference in molecular mass of the formed diazonium radicals, namely DAZ 1 - 123.11 g mol⁻¹, DAZ 2 - 108.14 g mol⁻¹, DAZ 3 - 147 g mol⁻¹. Although the electrode covered with DAZ 3 had the highest molar mass (147 g mol⁻¹), the deposition of DAZ 1 occurred more efficiently, probably due to the resonance effect of NO₂ group in contrast with inductive effect of Cl. While -NO₂ and -Cl are both electron withdrawing groups, they could destabilize the ring leading to the spontaneous electrochemical deposition. On the contrary, -OCH₃ is an electron donating group able to stabilize the aromatic ring that in return shows slow increase in electrochemical deposition vs. number of cycles (Figure 1 (E)).

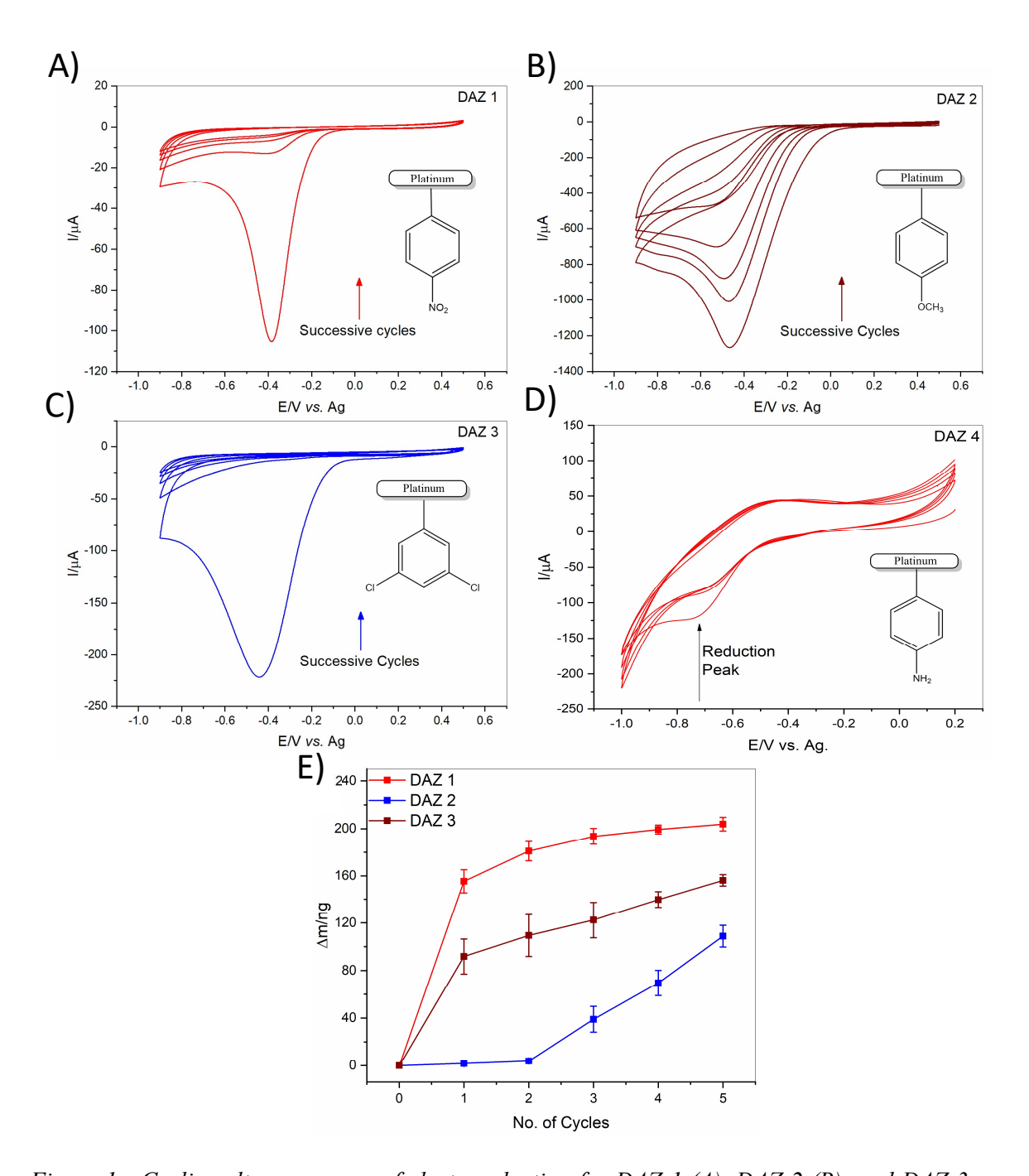
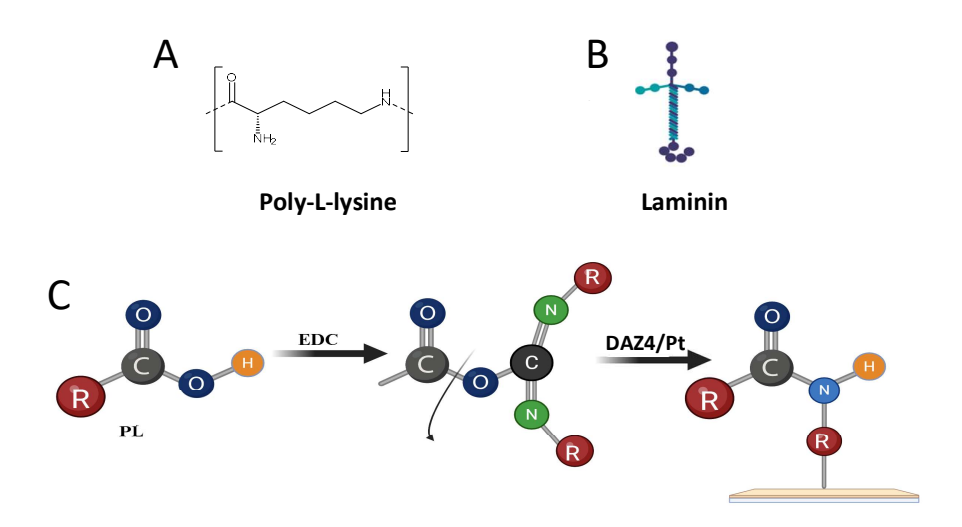


Figure 1 - Cyclic voltammograms of electroreduction for DAZ 1 (A), DAZ 2 (B), and DAZ 3 (C), and DAZ 1 further reduction to DAZ 4 (D) along with the EQCM data showing the mass deposition of DAZ 1, DAZ 2, and DAZ 3 with each successive cycle for 5 CV cycles (E).

Post-deposition, the modified surfaces were functionalized with poly-L-lysine (PL) to improve cellular adhesion. Two strategies were employed. First, a physical adsorption method was

implemented using drop-casting of 0.1% (w/v) PL solution. This led to uniform film coverage but with presumed limited long-term stability. In contrast, covalent immobilization was carried out on surfaces modified with amino-functionalized diazonium species using 1-ethyl-3-(3-dimethylaminopropyl)carbodiimide (EDC) as a coupling agent. This method enabled amide bond formation between carboxylic acid groups of PL and primary amines presented by the diazonium-modified surface, producing highly stable, bioactive films as shown in Scheme 1 [R2].



Scheme 1 – Chemical structure of poly-L-lysine (A) and Laminin (B). EDC coupling mechanism (C).

Surface changes following modification were confirmed by spectroscopic and morphological analysis. FTIR and Raman spectra (Figure 2 (A, B)) showed successful disappearance of diazonium-specific peaks (2000-2500 cm⁻¹) and emergence of new vibrational bands related to PL, C-C-N stretching (1280 cm⁻¹) and C=O stretching (1727 cm⁻¹). Furthermore, profilometry (Figure 2 (C)) revealed a noticeable increase in surface roughness after PL coupling, with DAZ 4 showing highest S_a values increasing from ~0.5 μm (bare diazonium layer) to ~2.1 μm for covalently grafted PL layers, which suggested film formation with increased texture. Wettability measurements supported these observations, with contact angle values decreasing from ~83° (bare platinum) to ~44° after PL deposition, confirming the hydrophilic nature of the peptide-rich coatings.

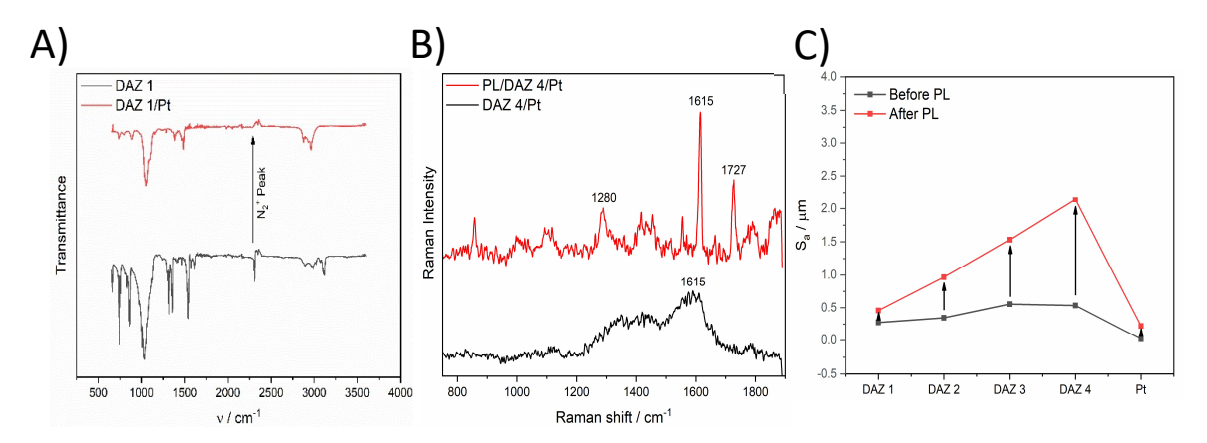


Figure 2 – Representative FTIR spectra of DAZ 1 showing the disappearance of a diazonium peak after electroreduction (DAZ 1/Pt) (A). Raman spectra of DAZ 4/Pt (black) and PL/DAZ 4/Pt (Red) with the marked peaks for DAZ 4 and PL (B). Surface roughness comparison for all samples before and after PL functionalization (C).

In vitro experiments with SH-SY5Y neuroblastoma cells demonstrated enhanced cell adhesion on the biofunctionalized electrodes. Platinum electrodes modified with electrografted diazonium salts supported markedly SH-SY5Y cell adhesion (between 250 and 550 cells mm⁻²) compared to unmodified Pt surfaces (from 100 to 200 cells mm⁻²) (Figure 3 (A)). Cells exhibited improved attachment and more uniform surface coverage on diazonium-coated substrates, especially those bearing terminal amine groups with the 3-fold increase in the cell attachment for DAZ 4 modified Pt surface (524 ± 19 cells mm⁻²). This enhancement is attributed to increased surface hydrophilicity and nanoscale roughness introduced by the aryl layers, which favour integrin-mediated adhesion^{25,26}. Nevertheless, cell morphology remained partially rounded and clustering was still observed (Figure 3 (C)), indicating that while diazonium grafting improves baseline biocompatibility, additional biochemical cues are needed to fully support neuronal spreading and network formation²⁷.

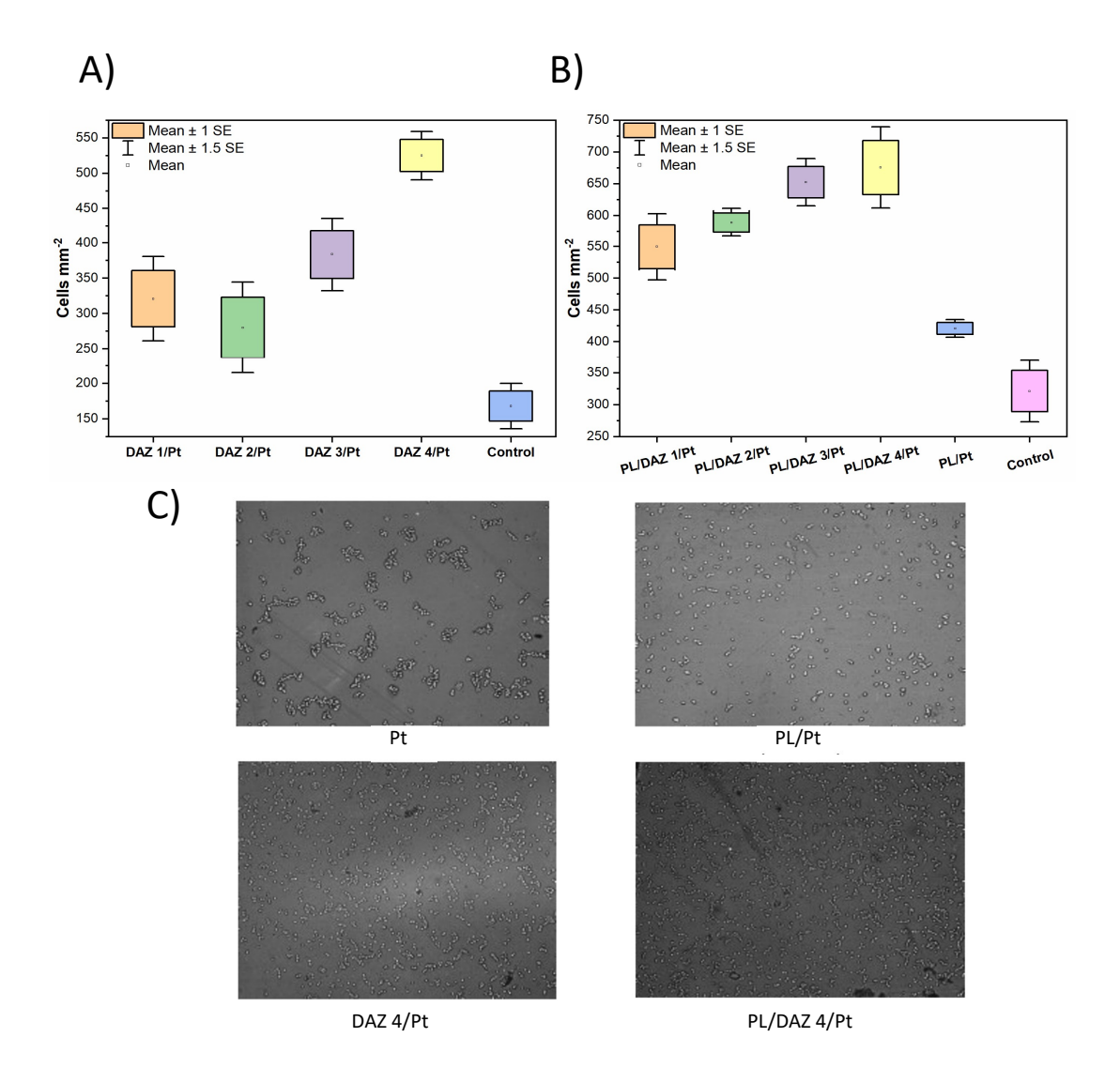


Figure 3 - Number of SH-SY5Y cells per mm² of sample attached to DAZ/Pt (A) and number of SH-SY5Y cells per mm² attached to PL-coated electrodes (B) with the box showing the range with standard error, with a square in the box representing the mean value. Representative cell culture images for the Pt, PL/Pt, DAZ 4/Pt and PL/DAZ 4/Pt samples (C).

To further enhance cellular adhesion and overcome the limitations of diazonium-only surfaces, poly-L-lysine (PL) was covalently immobilized onto the functionalized electrodes. PL promotes neuronal attachment through electrostatic interactions between its positively charged amine groups and negatively charged membrane components such as phospholipids and glycoproteins²⁸. Following PL grafting, SH-SY5Y cells exhibited enhanced spreading, more homogeneous distribution, features that were not observed on diazonium-only coatings (Figure

3 (C)). Quantitative cell imaging showed increases in cell number per mm² on the PL-modified electrodes compared to the untreated platinum, with PL/DAZ 4 showing the highest number of cells (700 ± 38 cells mm⁻²) when compared to PL/Pt (418 ± 26 cells mm⁻²) as shown in Figure 3 (B). Notably, PL coatings prepared via covalent coupling showed significantly higher confluency and individual cell spreading than those prepared via physical adsorption (Figure 3 (C)). These results demonstrated that diazonium-based modification, followed by site-specific peptide coupling, constitutes a powerful platform for tuning the cell-material interface of platinum electrodes²⁹ [R2].

The concept of applying diazonium salts coupled with bioactive molecules as biomedical coatings has been a subject of a patent application submitted into the Patent Office of the Republic of Poland under the title *Biofunctionalized organic coating*, *method of its preparation* and application; registration no. **P.442508**.

In this chapter, I demonstrated that combining electrografted diazonium monolayers with covalently immobilized poly-L-lysine enables the construction of a chemically stable and biologically responsive neural interface. Unlike conventional physisorbed coatings or polymer blends, this molecularly engineered platform offers precise control over interfacial functionality, allowing reproducible modulation of neuronal adhesion, morphology, and surface coverage. The results show that even bare diazonium layers improve cell adhesion over platinum, and that subsequent PL functionalization significantly amplifies this effect transforming the surface into a highly instructive and bioactive landscape. By systematically linking diazonium substituent chemistry, electrochemical behaviour, and cell response, this study delivers a transferable framework for designing advanced neural interfaces. It contributes broadly to materials science by bridging molecular-level surface engineering with functional neurobiological outcomes paving the way for next-generation implantable electrodes, biosensors, and bioelectronic platforms with tuneable biointegration and long-term performance.

4.1.2 Advancing neural selectivity through poly-L-lysine/laminin co-immobilization

To complement the broad electrostatic adhesion provided by poly-L-lysine, laminin was incorporated to introduce biological specificity into the surface design. While PL enhances initial attachment by interacting non-specifically with negatively charged cell membrane components, it does not engage cell-specific signalling pathways and may lead to heterogeneous or glial-like phenotypes. In contrast, laminin is an extracellular matrix protein that binds directly to neuronal integrins initiating intracellular signalling cascades that regulate cytoskeletal organization, neurite extension, and neuronal differentiation^{30,31}. These ligandreceptor interactions provide positional cues that promote axonal polarity and synaptic development, which are critical for forming functionally mature neurons^{32,33}. Co-immobilizing PL and laminin (LM) is expected to create a synergistic interface where PL promotes strong initial attachment, and laminin directs lineage-specific adhesion and outgrowth. This dualfunction surface thus better mimics the native neural extracellular environment and enables enhanced neural selectivity³⁴, improved morphological maturation, and reduced astrocytic spreading compared to PL alone³⁵. While drop-casting was initially considered for LM immobilization, I shifted to EDC-mediated coupling to achieve more stable and chemically anchored layers.

To achieve covalent immobilization of peptides, aminobenzene-functionalized electrodes were immersed in a 6 mM EDC solution prepared in PBS, containing either PL alone or a PL/LM mixture. After 20 minutes of incubation, the samples were rinsed with ultrapure water and airdried. This procedure facilitated amide bond formation between surface-exposed amine groups and the carboxyl moieties of the peptides, resulting in stable and biofunctionalized surfaces [R3].

Surface characterization confirmed the successful conjugation of both PL and LM. FTIR spectra of PL-modified surfaces (Figure 4 (A) inset) exhibited a distinguished CH₂ stretching modes in the range of 3050 cm⁻¹ – 2800 cm⁻¹. Upon laminin addition, additional peaks appeared at 1645 cm⁻¹ (C=O stretching) and 3380 cm⁻¹ (N-H stretching) (Figure 4 (B)), confirming successful co-immobilization of the ECM protein [R3]. Surface topography assessed by 3D optical profilometry (Figure 4 (C)) revealed a clear trend of increasing roughness: from 6.0 ± 1.7 nm on bare platinum to 19.1 ± 2.9 nm after aminobenzene modification, followed by 28.1 ± 2.6 nm and 35.3 ± 3.8 nm for PL and PL/LM functionalized electrodes, respectively. This progressive increase reflects sequential peptide layer formation and surface structuring.

Similarly, water contact angle measurements (Figure 3 (D)) showed a shift toward greater hydrophilicity, decreasing from $77 \pm 2^{\circ}$ for bare Pt to $60 \pm 1^{\circ}$ following aminobenzene grafting. $64 \pm 1^{\circ}$ Upon peptide conjugation, contact dropped further angles to 59 ± 2° aminobenzene/Polylysine/EDC (AB/PL/EDC) and for aminobenzene/Polylysine/Laminin/EDC (AB/PL/LM/EDC), which supported the formation of highly hydrophilic peptide coatings [R3].

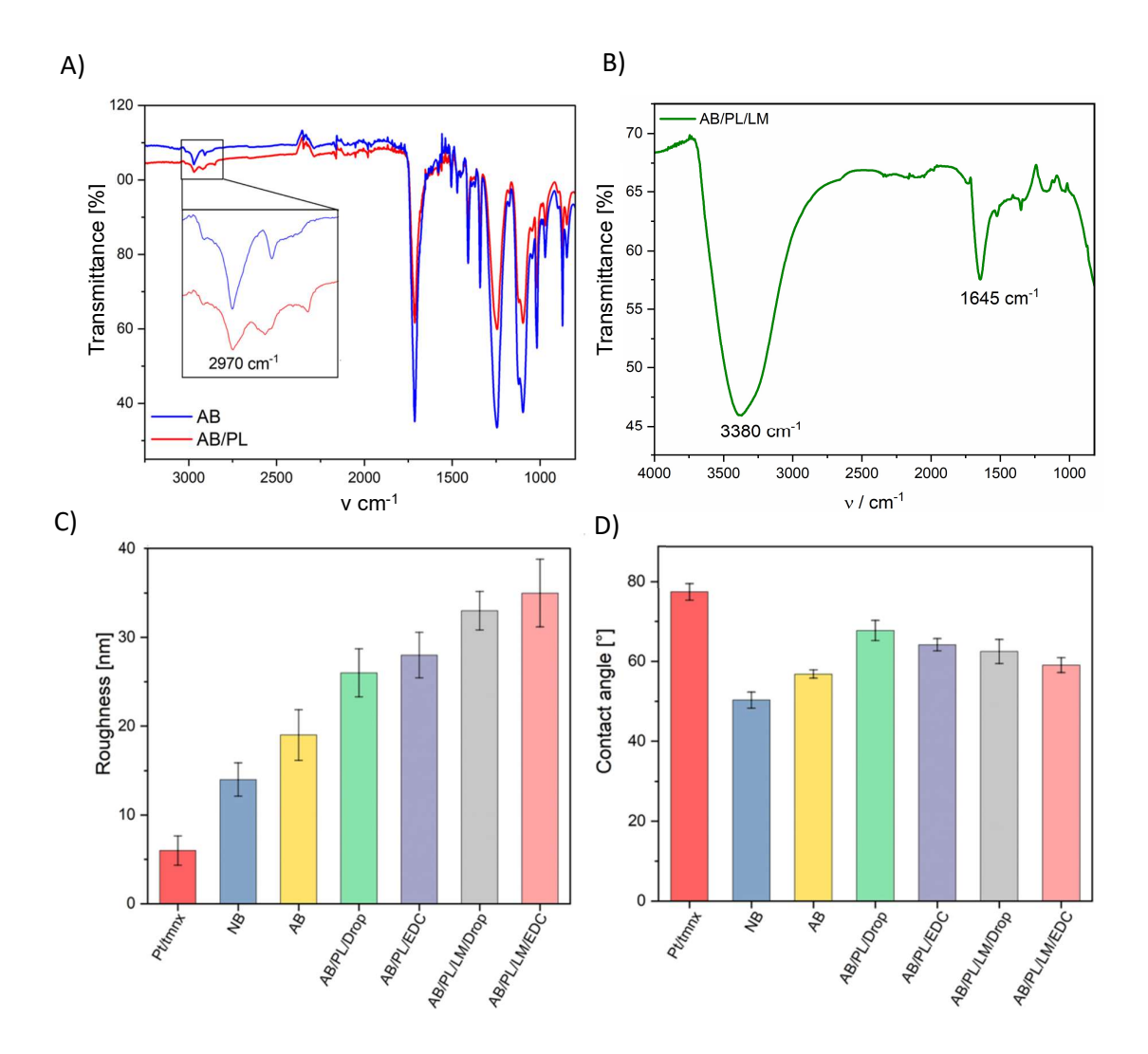


Figure 4 – FTIR spectra of AB and AB/PL with the inset of appearance of PL specific peak after functionalization (A) and LM specific peak (B), along with the change in roughness (C) and wettability (D) of the samples comparing the difference between drop casting and covalent immobilization of the polypeptides (PL and LM).

Next, I assessed adhesion of SH-SY5Y and U87 cells on the diazonium-modified electrodes. Cell density (Figure 5 (A, C)) on nitrobenzene (NB) and aminobenzene (AB) coatings increased to ~550 and ~750 cells mm⁻², respectively, which was significantly higher when compared with the tissue-culture plastic control (~300 cells mm⁻²). Adding polypeptides by drop-casting increased attachment further: AB/PL/Drop and AB/PL/LM/Drop supported ~800 and ~850 cells mm⁻², respectively. The biggest gains came from covalent co-immobilization: both AB/PL/EDC and AB/PL/LM/EDC approached ~1000 cells mm⁻², with AB/PL/LM/EDC reaching ~1100 cells mm⁻². Morphology analyses (Figure 5 (B)) showed that SH-SY5Y cells on AB/PL/LM/EDC displayed an N-type, neurite-bearing phenotype in ~60% of the population, while drop-cast coatings yielded only ~0-1.5% N-type cells. For U87 (Figure 5 (D)), the fraction of elongated (migratory) cells was high on AB alone (~63%) but fell to ~8% on AB/PL/LM/Drop; most cells there remained rounded and less motile.

Even without polypeptides, AB supported more attachment than NB (~750 vs ~550 cells mm⁻²), consistent with the higher biological affinity of amine-terminated aryl layers in buffered media (partial protonation, increased hydrogen-bonding capability) that favor early cell anchoring. Layering PL and laminin on AB amplified that effect; drop-cast films likely formed patchy, weakly adsorbed layers that can re-arrange or desorb, which explained why they lifted counts modestly (~800-850 cells mm⁻²) yet did not strongly shift phenotype. In contrast, EDC coupling created dense, covalently tethered "brush-like" polypeptides with many accessible binding motifs, boosting total adhesion (~1000-1100 cells mm⁻²) and selectively enriching neuronal features in SH-SY5Y. Mechanistically, PL contributed abundant cationic sites for electrostatic interaction with the negatively charged cell membrane³⁶, while laminin added integrin-binding domains³⁷ together and especially when immobilized via EDC these cues synergized to stabilize focal adhesion formation and neurite initiation.

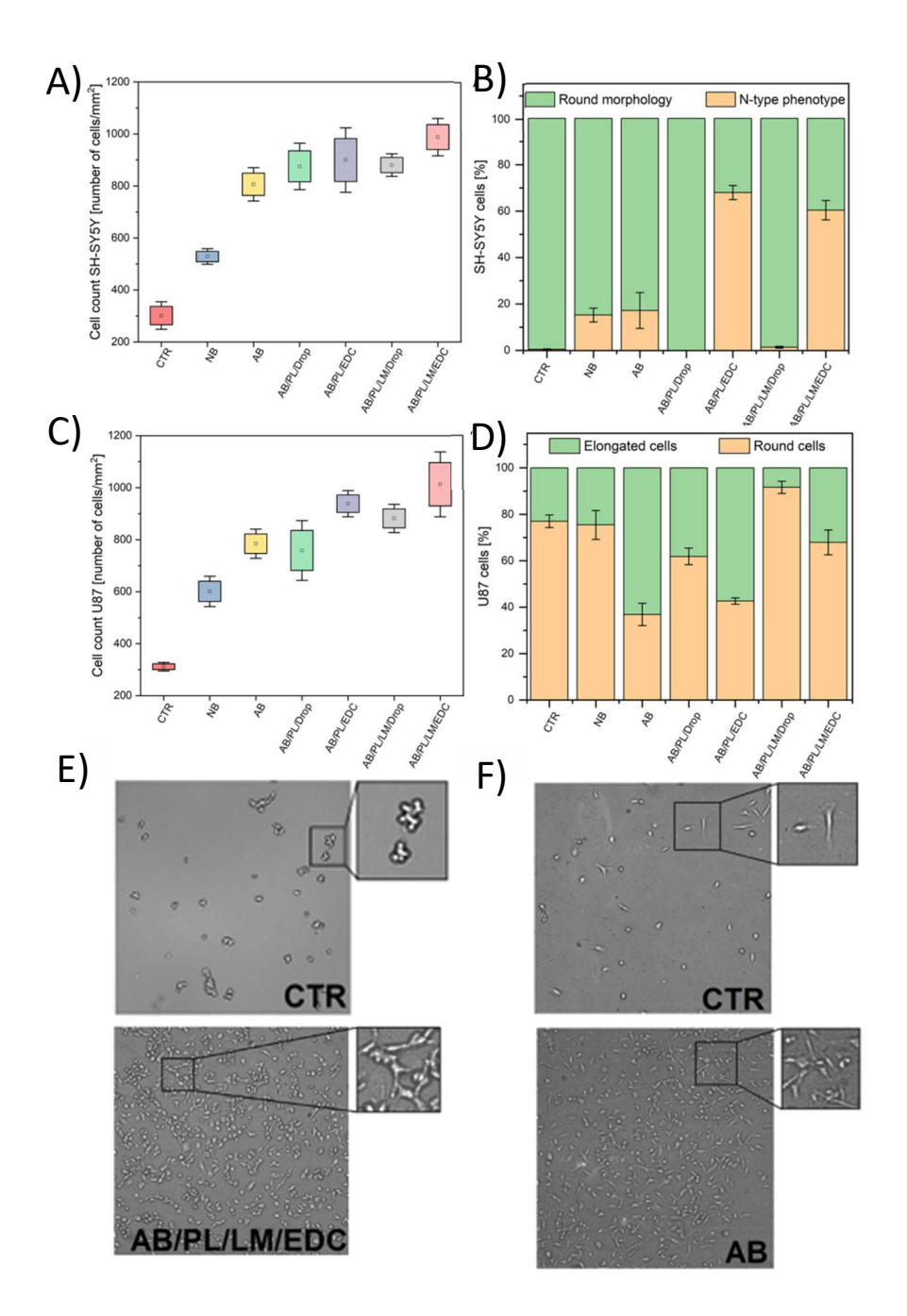


Figure 5 - Cell density of SH-SY5Y (A) and U87 cells (C) as number of cells per mm² for modified electrodes, compared to a tissue culture plastic control sample (CTR); a box represents a standard error with a mean value as a square in the centre of the box. Percentage of SH-SY5Y cells with a round and N-type phenotype (B). Percentage of U87 cells with elongate or round morphology (D). Representative optical images of SH-SY5Y cells cultured on a control sample and an electrode modified with AB/PL/LM/EDC (E). Representative optical images of U87 cells cultured on a control sample and an electrode modified with AB (F).

The increase from ~1.5% to ~60% SH-SY5Y N-type cells on AB/PL/LM/EDC indicated that stable, oriented laminin presentation together with PL's charge-based priming did more than just "stick" cells; it biased differentiation toward a neuron-like state with visible neurites as shown in (Figure 5 (E)). That is the most desirable phenotype for neural interfaces because it correlates with better neuronal contact and signal transduction³⁸. In parallel, U87 behavior shifted in the opposite, beneficial direction: the elongated (migratory) fraction was high on AB (~63%) but strongly suppressed on AB/PL/LM/Drop (~8%), pointing to reduced glial motility on laminin-containing coatings (likely due to strong, focal adhesion–stabilizing binding that discourages polarization and migration) (Figure 5 (F)). Together, these outcomes higher overall adhesion, more SH-SY5Y N-type cells, and fewer elongated U87 supported the central claim: EDC-mediated co-immobilization of PL/LM on diazonium-modified Pt improved biochemical presentation and surface microenvironments in a way that promoted neuron-specific attachment/differentiation while dampening glial motility key features for stable, functional neural interfaces.

Collectively, these results confirm that EDC-mediated co-immobilization of poly-L-lysine and laminin onto diazonium-modified platinum electrodes substantially improves surface biochemical and morphological properties. More importantly, it promotes neuron-specific adhesion and differentiation while suppressing glial cell mobility key features for the development of functional, biocompatible neural interfaces.

The concept of applying diazonium salts coupled with bioactive molecules as biomedical coatings has been a subject of a patent application submitted into the Patent Office of the Republic of Poland under the title *Polypeptide pro-adhesive coating and method of obtaining it; registration no.* **P.444427**.

In this chapter, I expanded the molecular engineering strategy established in the previous section by incorporating laminin, a biologically specific extracellular matrix protein alongside poly-L-lysine to create dual-functional neural biointerfaces. While PL enhanced general adhesion through electrostatic attraction, laminin introduced integrinmediated binding, triggering signalling pathways that drive neuronal differentiation and morphological maturation. Covalent co-immobilization of these peptides onto diazonium-grafted surfaces resulted in the formation of a hybrid coatings with both robust adhesion and high bioselectivity. The combined interface not only enhanced SH-SY5Y neuronal adhesion and neurite extension, but also reduced the migratory phenotype of U87

astrocytes, suggesting selective cellular guidance at the bioelectronic interface. By integrating synthetic surface chemistry with native extracellular signalling motifs, this work offered a versatile and biologically tuned strategy for constructing next-generation neural electrodes capable of modulating specific cellular behaviours and minimizing adverse glial responses. It further established a modular framework for customizing electrode interfaces at the molecular level to meet the complex demands of long-term neural integration.

4.2 Enhancing PEDOT:PSS adhesion and charge transfer by surface modification (R4)

Poly(3,4-ethylenedioxythiophene):polystyrene sulfonate (PEDOT:PSS) is one of the most widely adopted conducting polymers in bioelectronic applications due to its excellent electrical conductivity, mechanical flexibility, and compatibility with soft tissues^{39,40}. It has been successfully used for neural electrodes, biosensors, and organic electrochemical transistors that require efficient charge transfer and low inflammatory response^{41,42}. However, stabilizing PEDOT:PSS on metallic substrates such as platinum remains a major challenge: films often delaminate or crack under physiological conditions or during prolonged electrical stimulation due to weak interfacial adhesion^{43,44}. Prior strategies to enhance adhesion have included substrate roughening to increase mechanical interlocking, silane-based self-assembled monolayers, and diazonium-derived anchoring layers^{45,46}. Despite these efforts, most methods suffer from limitations such as harsh processing conditions or lack of long-term chemical stability.

Building on the insights from the previous chapters where electrografted diazonium layers were shown to improve cellular adhesion and interface stability, I hypothesized that a similar surface modification strategy could be applied to address the long-standing challenge of poor PEDOT:PSS adhesion to metallic substrates. In contrast to biological systems, where cell–surface interactions depend on biochemical cues, polymer–electrode interfaces require physicochemical compatibility, mechanical robustness, and long-term stability under electrochemical conditions. Diazonium salts have been widely applied to improve adhesion and long-term stability of polymer coatings on metal electrodes by forming robust, covalently bound aryl layers that resist delamination and degradation under physiological or electrochemical stress. Their electrografting can be performed under mild conditions, avoiding

the harsh thermal or chemical treatments required by some silane or plasma-based methods, while offering chemical versatility for further functionalization¹⁸.

Iodonium salts, on the other hand, offer additional benefits over diazonium ones, including higher stability, broader functional group tolerance, and efficient surface coupling without the need for in situ diazotization⁴⁷. Notably, electrografted iodonium salts have yet to be explored as adhesion-promoting layers for conducting polymers. Therefore, in the next part of my work, iodonium-based interlayers were chosen to provide a more stable and controllable adhesion-promoting platform for PEDOT:PSS on platinum, enabling durable coatings without compromising electrochemical performance. By combining organic surface chemistry with conducting polymer integration, my study aimed to develop a modular and scalable platform that enhanced the structural and electrical performance of neural bioelectronic interfaces.

Consequently, I selected four commercially available iodonium salts with distinct structural features to investigate their effect on PEDOT:PSS adhesion and electrochemical performance. These included: bis(4-tert-butylphenyl)iodonium hexafluorophosphate (Salt A), (4nitrophenyl)(2,4,6-trimethylphenyl)iodonium triflate (Salt B), diphenyliodonium chloride (Salt C), and bis(4-methylphenyl)iodonium hexafluorophosphate (Salt D). Each salt was chosen to represent different steric and electronic environments at the aryl iodide core, which influenced the grafting efficiency, interfacial stability, and compatibility with conducting polymers. Salt A bears bulky tert-butyl groups that introduce steric hindrance; Salt B includes a strong electronwithdrawing nitro group, which may modulate the reactivity of the aryl radical formed during electrografting. Salt C, being water-soluble and unsubstituted, allowed electrografting to be performed in an aqueous medium, which is more environmentally friendly, cost-effective, and safer than conventional organic solvent systems typically required for diazonium or iodonium salts which served as a simple benchmark for comparison, while Salt D, with para-methyl substituents, introduces mild electron-donating effects, offering insight into how small alkyl groups affect polymer interface performance. This structural diversity enabled a systematic evaluation of how aryl substitution influences electrografting behaviour and PEDOT:PSS anchoring properties.

The selected salts were electrografted onto platinum-coated Thermanox substrates using cyclic voltammetry. The conditions were tuned based on each salt's solubility and redox potential; for instance, Salt C was deposited in aqueous KNO₃, while others used *t*Bu₄NPF₆ in acetonitrile. During CV, a cathodic peak indicated the electrochemical reduction of the iodonium cation,

leading to homolytic cleavage of the I-C bond and formation of reactive aryl species that covalently attached to the platinum surface (Figure 6 (A, B, C, D)).

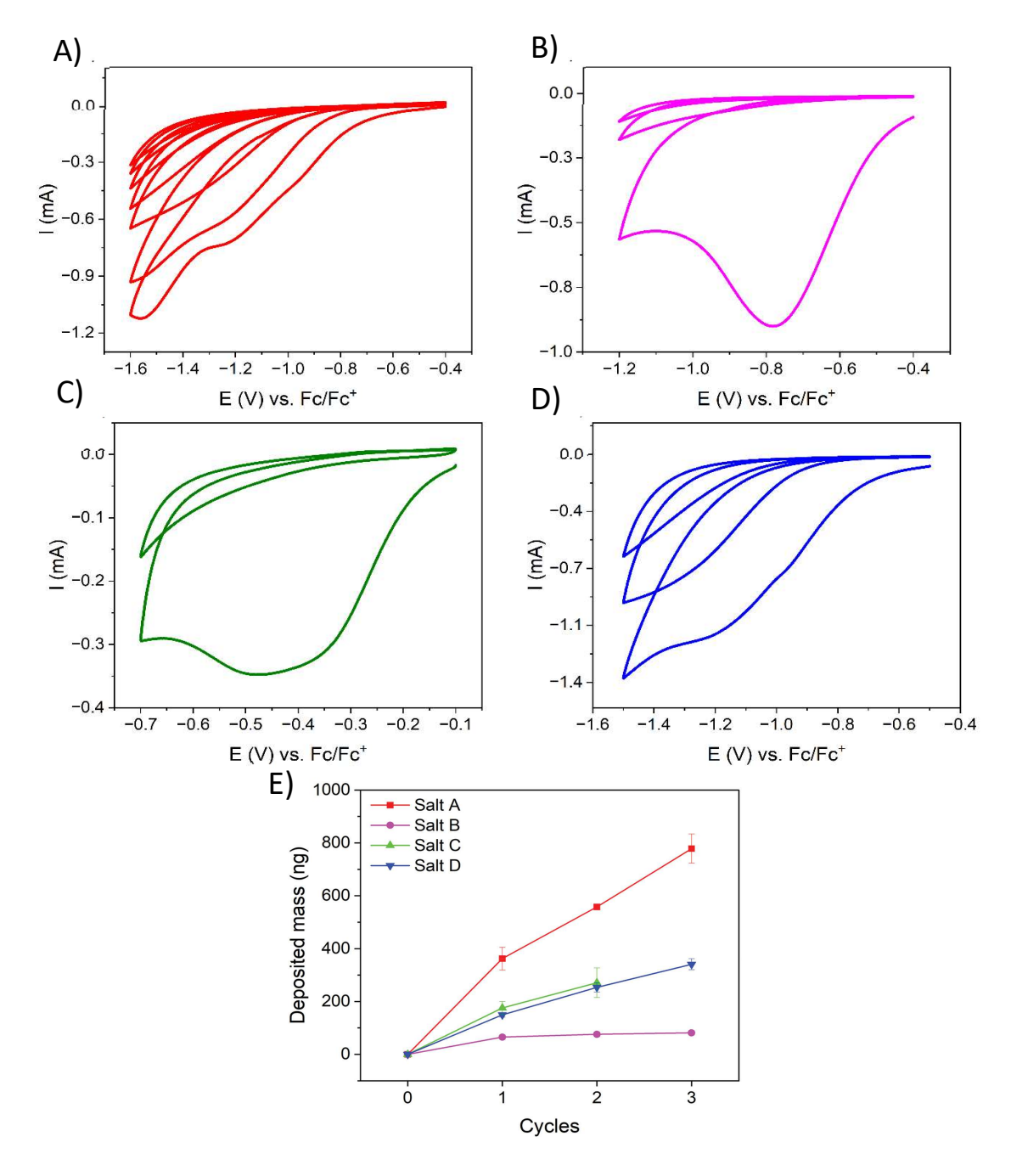


Figure 6 - Cyclic voltammograms of the process of electroreduction of iodonium salts: (A) bis(4-tertbutylphenyl) iodonium hexafluorophosphate (Salt A), (B) (4-nitrophenyl)(2,4,6-trimethylphenyl)iodonium triflate (Salt B), (C) diphenyliodonium chloride (Salt C) and (D) bis(4-methylphenyl)iodonium hexafluorophosphate (Salt D), changes in mass deposited on the electrode with respect to CV cycles for Salt (A, B, C, D) derived by EQCM results (E).

Different potential windows were applied for Salts A–D to achieve efficient electrodeposition, with electroreduction occurring at –1.2 V vs. Fc/Fc⁺ for Salt A, –0.8 V vs. Fc/Fc⁺ for Salt B, –0.4 V vs. Fc/Fc⁺ for Salt C, and –1.1 V vs. Fc/Fc⁺ for Salt D. Salt C displayed the least negative reduction potential, which was attributed to the aqueous medium used for its deposition and the presence of an unsubstituted aromatic ring. For Salt B and Salt C, electroreduction was completed within a single CV cycle, as no reduction peak appeared in subsequent scans. This behaviour was consistent with rapid electrode passivation, in which an organic film formed on the surface prevented further electrochemical reaction. In contrast, reduction peaks for Salt A and Salt D persisted in later cycles, though they shifted slightly toward more negative potentials and exhibited lower current intensity. This suggested that the aryl radicals generated during electroreduction could undergo further reduction to yield aryl anions, as previously reported⁴⁸.

The reduction potentials for iodonium salts were approximately 0.5 V more negative than for their diazonium analogues, reflecting the greater intrinsic stability of the I-Ar bond. Iodine's larger covalent radius and more diffuse electron density stabilize the positive charge on the iodine center, making the bond less susceptible to cleavage⁴⁹. While this stability required higher overpotentials for electrografting, it also improved handling safety by avoiding the rapid, uncontrolled decomposition that can occur with some diazonium salts¹⁹. Iodonium salts underwent one-electron electroreduction process similar to that of diazonium salts: the cation was reduced to form an aryl radical, which covalently bound to the electrode surface while the counter fragment was released into solution. High reactivity of iodonium species led to multilayer growth, especially when more than one CV cycle was applied. For the unsymmetrical Salt B, cleavage could occur at either aromatic ring, although steric hindrance meant that only the nitro-substituted aryl group could be deposited effectively^{50,51}. Asymmetric iodonium salts in general can generate radicals from both aryl groups, which may compete for surface attachment. High regioselectivity can be achieved using methods such as plasmonassisted transformations⁵²; in the case of Salt B, regioselectivity was promoted by methyl substituents at the 2, 4, and 6 positions of one phenyl ring, which steered the reaction toward a single attachment pathway as shown in Scheme 2.

Scheme 2 - Mechanism of bond cleavage, aryl radical formation and attachment of the radical to the Pt electrode for Salt B. Mechanism pathway 2 shows the actual process taking place during the electroreduction.

To evaluate the efficiency of surface grafting, I performed electrochemical quartz crystal microbalance (EQCM) measurements during the electrografting of each iodonium salt onto EQCM gold resonator (Figure 6 (E)). The electroreduction was carried out via cyclic voltammetry at a scan rate of 50 mV s⁻¹ within salt-specific potential ranges. EQCM revealed distinct mass gains reflecting differences in grafting efficiency: Salt A showed the highest deposition mass (778.3 \pm 55.1 ng), followed by Salt D (340.6 \pm 20.8 ng), Salt C (270.7 \pm 56.1 ng), and Salt B (81.3 \pm 7.8 ng). These disparities were attributed to the differing reactivity and steric accessibility of the generated aryl radicals during electroreduction. Notably, Salt B, containing a para-nitrophenyl substituent, yielded the lowest mass due to the deactivating effect of the electron-withdrawing nitro group⁵³.

The differences in roughness (Figure 7 (A)) and wettability (Figure 7 (B)) that I observed between the iodonium-modified electrodes were closely related to the molecular structure of the grafted salts and their packing behaviour on the platinum surface. The substantial increase in roughness for Salt A ($S_a = 0.35 \pm 0.07 \mu m$) was consistent with the bulky tert-butyl substituents, which introduced steric hindrance during film growth. I believed that this steric effect disrupted uniform packing of the aryl radicals, producing a more irregular and textured surface. Such a morphology was likely advantageous for PEDOT:PSS adhesion, as the increased surface area and micro-scale asperities could promote mechanical interlocking of the polymer film⁵⁴. In contrast, the extremely low roughness for Salt D ($S_a = 0.04 \pm 0.01 \mu m$) suggested that the smaller methyl groups allowed for closer packing and more compact, uniform layer formation. While smoother surfaces generally reduced opportunities for mechanical anchoring, I considered that the more ordered organic layer from Salt D could improve chemical compatibility and electronic coupling with the polymer⁵⁵.

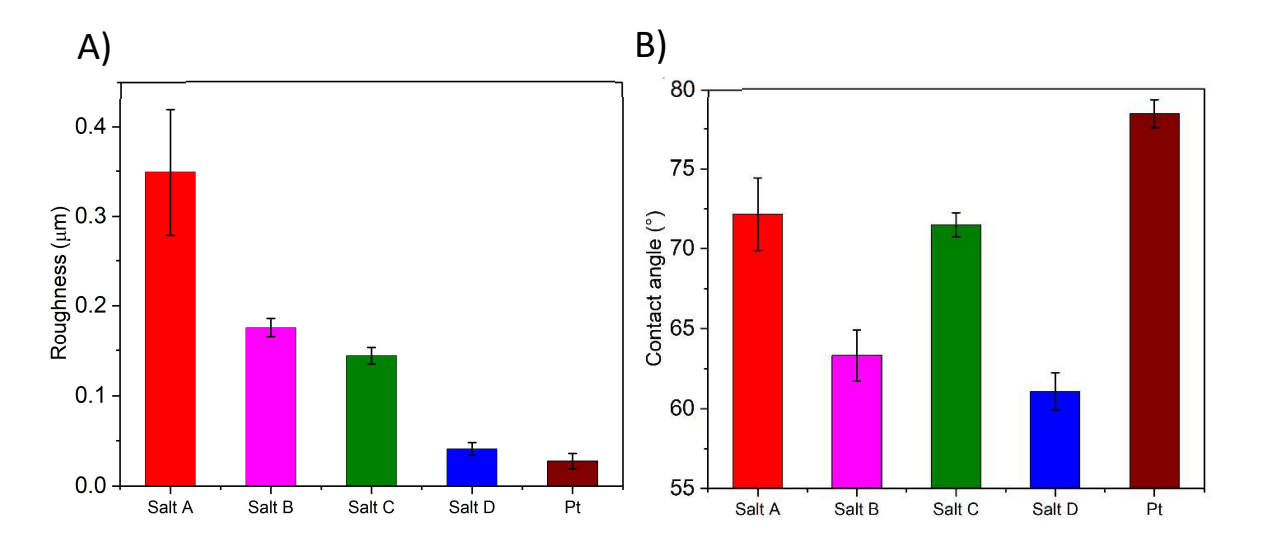


Figure 7 - Roughness (A) and wettability (B) analysis of electrode surfaces modified with electrodeposited iodonium salts compared with a bare Pt electrode.

The wettability results (Figure 7 (B)) supported this interpretation. All grafted surfaces displayed improved hydrophilicity compared to bare platinum (contact angle $78 \pm 1^{\circ}$), indicating that the introduction of the organic layer altered the surface energy. The lowest contact angle for Salt D ($61 \pm 1^{\circ}$) suggested that its compact, possibly more polarizable film presented a surface chemistry highly favourable to the aqueous PEDOT:PSS dispersion, enabling uniform wetting and film formation. Salt B, which contained a strongly electron-

withdrawing nitro group, also reduced the contact angle ($63 \pm 2^{\circ}$), likely due to increased surface polarity; however, its lower grafting mass may have limited the long-term adhesion improvement. I considered improved wettability to be critical for PEDOT:PSS deposition, as it minimized void formation at the interface and facilitated better polymer chain alignment during drying.

Electrochemical impedance spectroscopy (EIS) was used to evaluate the effect of electrodeposited iodonium salts on the conductivity and capacitance of Pt electrodes. Bode plots (Figure 8 (A)) revealed that all modified electrodes exhibited impedance profiles similar in shape to bare Pt, confirming that the coatings did not compromise conductivity. Phase angle plots (Figure 8 (B)) showed a single peak between 1–10 Hz for all samples, indicative of capacitive behaviour dominated by a single time constant. The experimental data were fitted using a modified Randles circuit consisting of solution resistance (R_s), constant phase element (CPE), charge transfer resistance (R_{CT}), and Warburg diffusion element (W). Compared with bare Pt ($R_{CT} = 12.3 \pm 0.7 \text{ k}\Omega$; $C = 42.2 \pm 0.1 \mu\text{F}$), all coated electrodes exhibited increased R_{CT} values, confirming the formation of an organic barrier layer that partially blocked electron transfer. The most pronounced increase was observed for Salt C ($R_{CT} = 450.9 \pm 78.8 \text{ k}\Omega$) and Salt D ($R_{CT} = 61.7 \pm 1.4 \text{ k}\Omega$). The CPE exponent (n) approached 1 in all cases, consistent with nearly ideal capacitive behaviour. Capacitance values calculated from CPE parameters varied significantly between coatings, with the highest for Salt B (693.5 \pm 0.1 μ F) and the lowest for Salt D (30.4 \pm 0.2 μ F), the latter being slightly below the bare Pt value (42.2 \pm 0.1 μ F), indicating that the specific iodonium salt chemistry strongly influenced interfacial charge storage characteristics.

EIS analysis after PEDOT:PSS coating (Figure 8 (C, D)) further revealed the functional significance of these surface modifications. The charge transfer resistance (R_{CT}) of PEDOT:PSS-coated electrodes decreased markedly after iodonium grafting, from $100 \pm 8.9~\Omega$ for unmodified Pt to $16.8 \pm 0.6~\Omega$ for Salt D and $8.1 \pm 1.0~\Omega$ for Salt A. I attributed this improvement to the enhanced physical and electronic contact between the polymer and the modified surface. For Salt A, the increased roughness and favourable electronic effects from its substituents may have provided additional pathways for charge transport. For Salt D, the smoother, highly wettable interface likely supported the formation of a continuous PEDOT:PSS layer with fewer defects, leading to lower impedance. These findings were consistent with previous studies reporting that interlayers with optimized surface energy and morphology could

simultaneously improve mechanical stability and electrochemical performance of conducting polymers in bioelectronic applications^{56,57}.

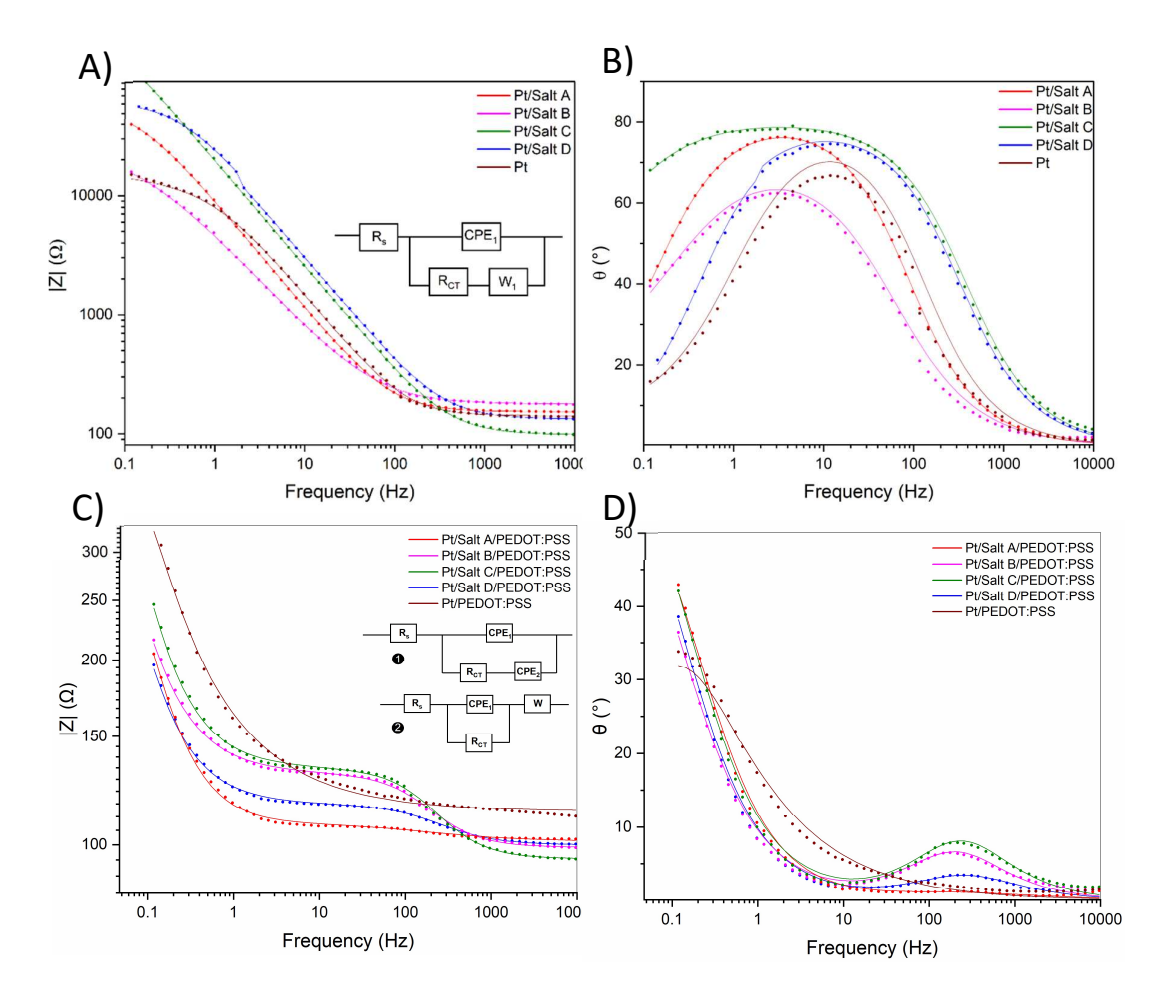


Figure 8 - EIS data in the form of Bode plots of Pt electrodes modified with iodonium organic layers: impedance module vs. frequency (A) with the circuit as a inset, phase angle vs. frequency (B). EIS plots after PEDOT:PSS deposited on Pt electrodes modified with organic layers: impedance module vs. frequency (C), with the circuits Pt/Salt/PEDOT:PSS [1], Pt/PEDOT:PSS [2]; phase angle vs. frequency (D). Experimental data are presented as dots, while simulated spectra are presented as solid lines.

After electrografting the iodonium salts, I deposited PEDOT:PSS onto the modified platinum electrodes and found clear evidence that the underlying interlayer chemistry influenced the polymer's electrochemical properties. The substantial increases in charge storage capacity (CSC) for Pt/Salt B/PEDOT:PSS (67.0 mC cm⁻²) and Pt/Salt D/PEDOT:PSS (70.9 mC cm⁻²), compared with 45.8 mC cm⁻² for unmodified Pt/PEDOT:PSS, suggested that the grafted aryl

layers improved both the effective electroactive surface area and the efficiency of ion penetration into the PEDOT:PSS network. I considered that this enhancement arose from the improved film continuity and reduced interfacial defects achieved when the polymer was cast onto a chemically compatible, covalently bound organic layer. The wettability gains measured earlier, particularly for Salt B and Salt D, likely promoted better spreading of the aqueous PEDOT:PSS dispersion, ensuring more uniform coating and tighter interfacial contact. A denser and more conformal polymer layer would increase the number of accessible redox sites, thereby elevating CSC.

To assess the long-term stability of the PEDOT:PSS coatings, I performed a 30-day aging study in PBS at room temperature, followed by UV-Vis analysis of the incubation solutions (Figure 9 (A)). For unmodified Pt/PEDOT:PSS electrodes, the UV-Vis spectra showed pronounced absorbance peaks at 268 nm and 325 nm, corresponding to the leaching of PSS and PEDOT chains, respectively. In contrast, electrodes modified with iodonium salts, particularly Salt B and Salt D, exhibited markedly lower absorbance intensities at both wavelengths. Quantitatively, the 325 nm peak intensity was reduced by approximately 50% for Pt/Salt B/PEDOT:PSS and 70% for Pt/Salt D/PEDOT:PSS compared to the control, indicating significantly less PEDOT loss during immersion. This suppression of polymer release demonstrated that the covalently bound iodonium interlayers effectively anchored the PEDOT:PSS film, limiting chain detachment and dissolution under physiological conditions⁵⁸.

Ageing studies on PEDOT:PSS-coated electrodes demonstrated that iodonium-derived interlayers enhanced the long-term capacitance stability of polymer (Figure 9 (B, C)). The unmodified Pt/PEDOT:PSS electrode exhibited the highest CSC loss (53.5%), confirming its poor stability, whereas the presence of organic layers particularly those formed from Salt C and Salt D significantly reduced capacitance degradation, consistent with UV-Vis stability results. Notably, Pt/Salt D/PEDOT:PSS showed a 20% increase in capacitance after ageing, likely due to microstructural crystallinity and morphological changes during aqueous immersion. Tape test observations further supported the stabilizing role of these interlayers, with improved adhesion of PEDOT:PSS on all modified surfaces except Pt/Salt C/PEDOT:PSS, where localized delamination occurred at the immersion site during electrografting, indicating weaker interfacial bonding^{59,60}.

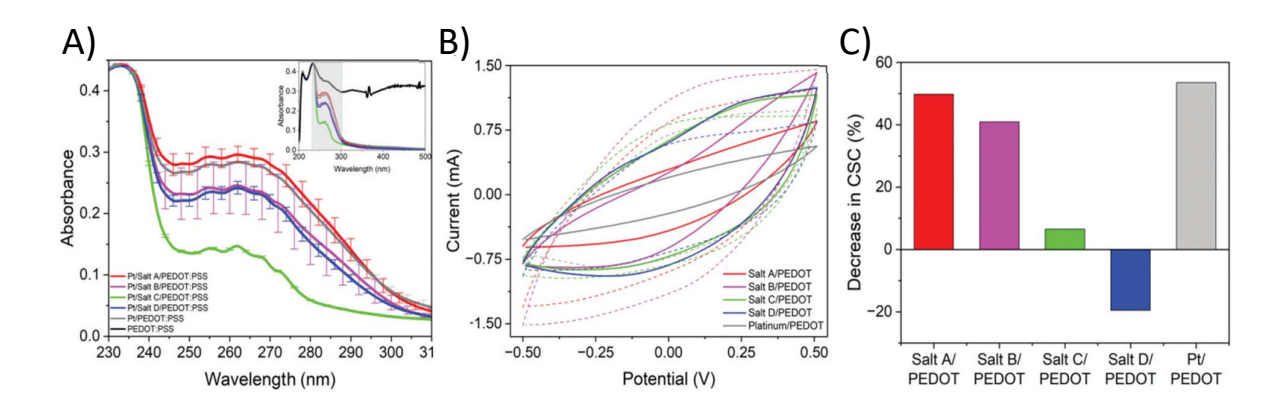


Figure 9 - UV-Vis spectra of PBS solution after 30 days of ageing in the spectral region from 230 nm to 310 nm; inset: UV-Vis spectra of PEDOT:PSS in the range from 220 nm to 500 nm (A); CV curves for samples after ageing (solid lines) and before (dashed lines) at scan rate = 100 mV s^{-1} (B); Decrease in CSC values at scan rate = 100 mV s^{-1} for samples after 30 days of ageing test (C).

The mechanical robustness of the coatings was further evaluated by tape adhesion tests. On bare Pt/PEDOT:PSS electrodes, the polymer layer was visibly removed upon peeling, confirming weak interfacial adhesion. In contrast, PEDOT:PSS films deposited on Salt B- and Salt D-modified electrodes remained intact, with no visible detachment. Raman spectroscopy performed after tape removal supported these observations: the characteristic PEDOT vibrational modes, such as the $C\alpha$ = $C\beta$ symmetric stretching at ~1446 cm⁻¹ and the C-O-C deformation at ~1256 cm⁻¹, were still present for Pt/Salt B/PEDOT:PSS and Pt/Salt D/PEDOT:PSS samples but were largely absent in the unmodified control.

I interpreted these results as evidence that the iodonium interlayers improved coating stability through both chemical and physical mechanisms. The formation of strong Pt–C covalent bonds provided a robust chemical anchor, while the tailored surface chemistry of Salt B and Salt D enhanced polymer wetting, reducing microvoids at the interface where delamination could initiate. Salt D's combination of high wettability and compact, defect-minimized grafted layer likely explains its superior retention of PEDOT compared to Salt B, even though both significantly outperformed the control.

The concept of improved adhesion of PEDOT:PSS is a patent gained and registered to the Patent Office of the Republic of Poland under the title *Method for obtaining pro-adhesive layer;* registration no. **P.447109**.

This chapter established a new paradigm in conducting polymer-electrode integration by introducing electrografted aryl iodonium salts as molecular anchoring layers for PEDOT:PSS. Through systematic electrochemical, spectroscopic, and mechanical analyses, I showed that these ultrathin organic interlayers drastically improve PEDOT:PSS adhesion, stability, and charge transport overcoming one of the most persistent limitations in organic bioelectronics. Unlike conventional surface treatments, which often suffer from poor reproducibility, chemical instability, or substrate specificity, iodonium-based grafting offers a modular, chemically controlled, and substratecompatible strategy for building high-performance interfaces. The results not only demonstrated that interfacial adhesion can be molecularly engineered using iodonium precursors but also provided mechanistic insight into how surface chemistry dictates polymer cohesion, degradation resistance, and electrochemical function. This work expanded the utility of iodonium chemistry from surface patterning to polymer anchoring, and marks a critical advancement toward durable, electrically efficient, and biologically stable neural electrodes bridging the gap between molecular interface design and functional device reliability.

4.3 Mixed thiol self-assembled monolayers for neural interface engineering (R5)

To complement my electrografted coatings, I investigated an alternative, self-assembling surface modification method based on thiol-gold chemistry. Self-assembled monolayers (SAMs) of alkanethiols on gold are well-established platforms for tailoring interfacial properties at the molecular level, offering precise control over surface chemistry, wettability, and charge all critical factors for modulating neural cell behaviour 13 . In this part of my work, I selected two structurally distinct thiols, 2-thiophenethiol (TT) and 2-mercaptoethanol (ME), to create mixed SAMs with tuneable biointerface properties. TT, featuring an aromatic thiophene ring, is relatively hydrophobic and π -conjugated, providing a planar, electron-rich scaffold that may influence protein adsorption and electrochemical interactions 61 . In contrast, ME contains a hydrophilic hydroxyl group, promoting hydrogen bonding and increased surface wettability, which can enhance neuronal adhesion and reduce astrocytic activation. By varying the TT:ME ratio, I aimed to explore how hydrophilic—hydrophobic balance and functional group diversity affect surface morphology, charge-transfer behaviour, and ultimately the biological response of mixed neuron-glia cultures. This design addresses a key knowledge gap in literature:

although individual thiol SAMs have been studied for biosensing and anti-fouling applications, the combinatorial effects of blended SAMs on neural tissue integration remain underexplored. The present work provides a systematic framework for evaluating such interactions on gold neural electrodes.

I modified gold-coated Thermanox substrates with mixed self-assembled monolayers (SAMs) of 2-thiophenethiol (TT) and 2-mercaptoethanol (ME) at volumetric ratios of 1:0, 1:0.5, 1:1, 0.5:1, and 0:1. I performed cyclic voltammetry (CV) to evaluate the electrochemical behaviour of bare and thiol-modified gold surfaces prepared with different ratios of 2-thiophenethiol (TT) and 2-mercaptoethanol (ME) (Figure 10 (A)). The bare Au control exhibited a broad anodic peak at approximately +1.2 V and a broad cathodic feature near 0.5 V, which were characteristic of gold oxidation and reduction, respectively. The disappearance of these peaks in the modified samples confirmed that I had successfully functionalized the gold surfaces⁶². The TT-only sample (1:0) showed reduced faradaic currents at both potentials, indicating that the bulky thiophenethiol groups formed a compact layer that hindered electron transfer and protected the gold from oxidation. The samples containing both TT and ME (1:0.5, 0.5:1, 1:1) displayed even lower faradaic currents, as the combination of molecules still produced a densely packed structure that further restricted charge transfer; although ME was smaller than TT, it still contributed to surface crowding. In contrast, the ME-only sample (0:1) produced the highest faradaic current, which I attributed to catalytic oxidation of ME at high positive potentials (1.2 V vs. Ag/AgCl) to a sulfidoacetic acid monolayer⁶³. Charge storage capacity (CSC) analysis (Figure 10 (B)) reflected these trends: the bare Au surface exhibited 10.4 ± 0.8 mC cm⁻², TTrich surfaces showed reduced values (1:0 = 7.9 ± 0.6 mC cm⁻²; 1:0.5 = 3.9 ± 0.4 mC cm⁻²; $0.5:1 = 3.8 \pm 0.3 \text{ mC cm}^{-2}$), and the 1:1 mixture gave a moderate CSC ($5.3 \pm 0.6 \text{ mC cm}^{-2}$). The ME-only surface (0:1) reached the highest CSC (21.9 ± 1.0 mC cm⁻²), consistent with its additional faradaic contribution.

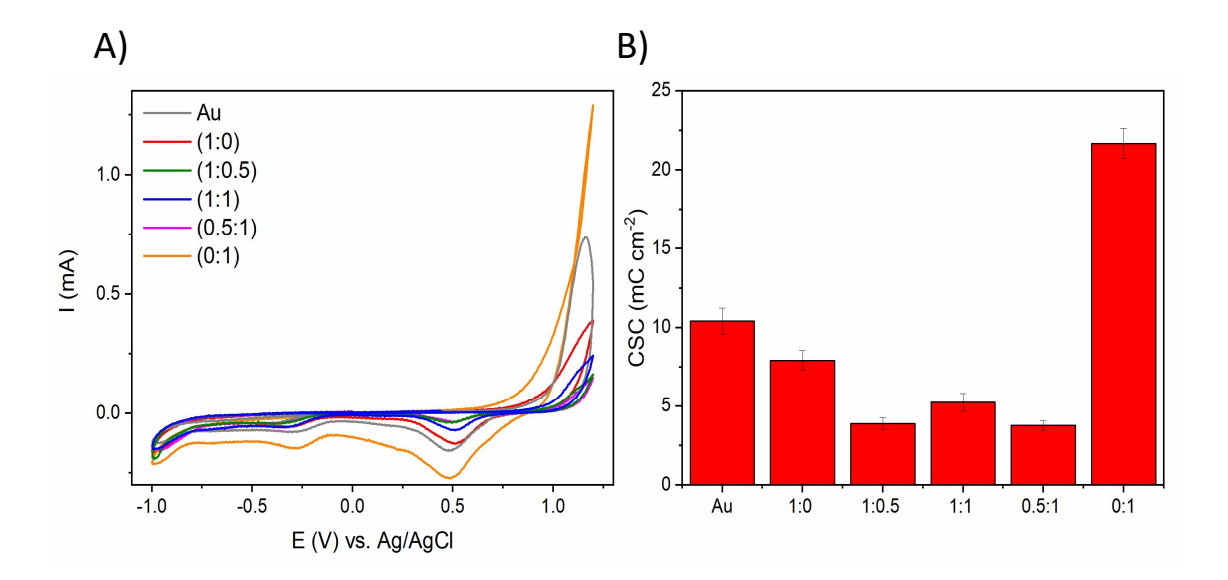


Figure 10 - CV curves (A) and corresponding charge storage capacity (CSC) values (B) of bare Au surfaces as well as Au surfaces modified with the mixture of TT and ME in different proportions (1:0, 1:0.5, 1:1, 0.5:1, 0:1). CV were collected in PBS at the scan rate of 100 mV s^{-1} .

I conducted AFM analysis to investigate how thiol functionalization influenced the surface morphology of gold substrates (Figure 11 (A)). Surface roughness measurements (Figure 11 (B)) revealed marked changes in texture following modification. The unmodified Au surface exhibited the highest S_a value (7.37 \pm 0.61 nm) and displayed large gold particulate features averaging 84.58 ± 1.89 nm in diameter, indicative of substantial surface heterogeneity likely caused by minimal molecular organization or spontaneous aggregation in the absence of a stabilizing coating⁶⁴. Surfaces coated solely with TT (1:0) showed similarly large particulates $(113.43 \pm 3.22 \text{ nm})$, reflecting pronounced aggregation from strong intermolecular interactions and limited lateral packing efficiency, consistent with literature reports for pure TT monolayers⁶⁴. As the TT:ME ratio shifted toward 1:1, the roughness decreased slightly to 4.54 \pm 0.38 nm, with mixed-ratio coatings (1:0.5 and 1:1) exhibiting smaller particle sizes (35.17 \pm 1.46 nm and 56.12 ± 2.34 nm, respectively) and improved packing density. This suggested that ME disrupted strong TT-TT interactions, reducing aggregation and enabling more compact, uniform monolayers. Increasing the ME content further reduced roughness to 0.34 ± 0.03 nm (0.5:1) and 0.32 ± 0.03 nm (0:1), eliminating visible particulates. This substantial smoothing effect was attributed to ME's ability to form stable Au-S bonds while its hydroxyl group

enabled hydrogen bonding, promoting uniform deposition and multilayer organic structures^{65,66}. Overall, the data showed that thiol composition critically influenced nanoscale morphology ranging from large, irregular particulates in ME-free coatings (Au, 1:0) to densely packed, uniform structures at intermediate ME levels (1:1, 1:0.5), and nearly atomically smooth surfaces at higher ME contents (0.5:1, 0:1).

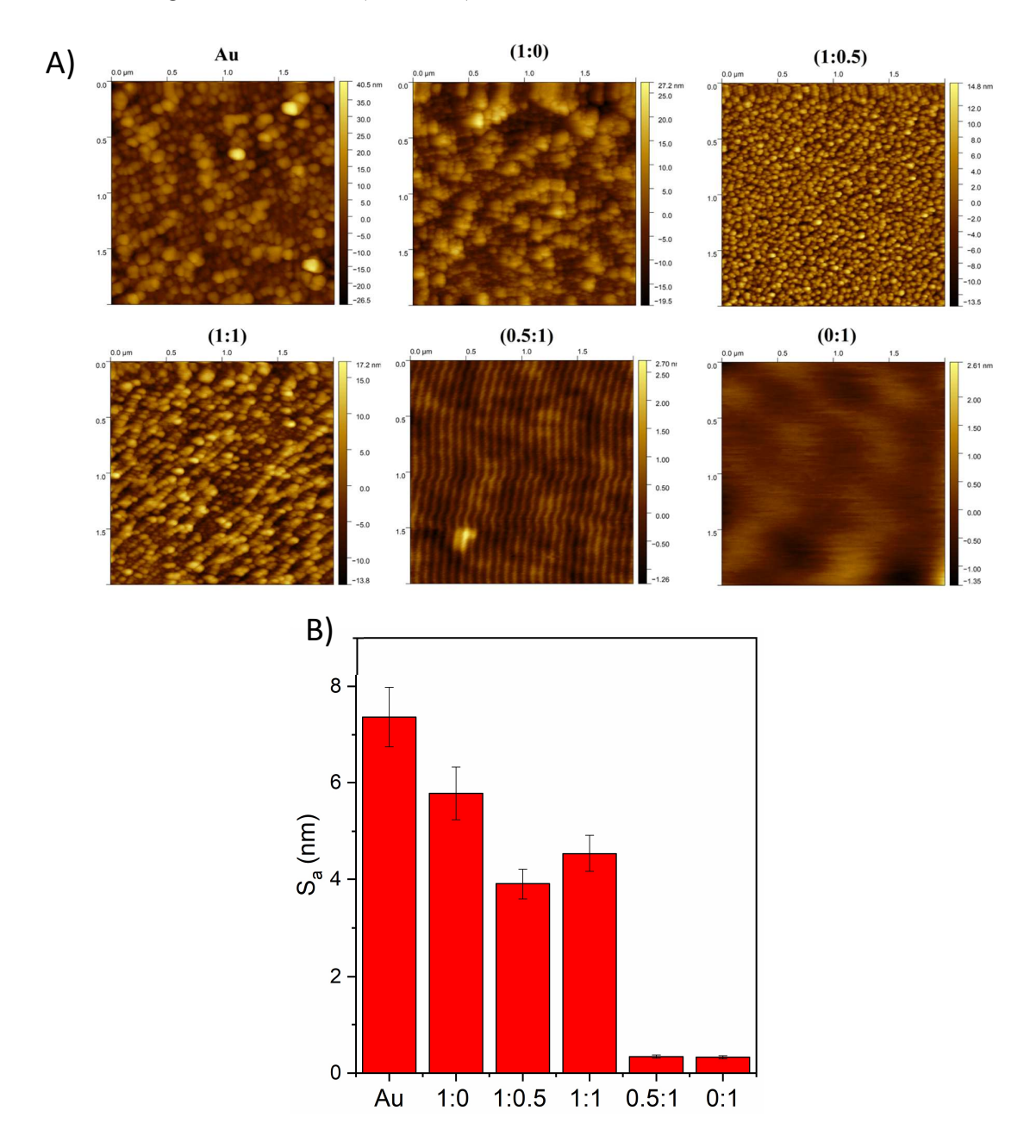


Figure 11 - AFM images (A), surface roughness S_a (B) of unmodified Au surfaces as well as Au surfaces modified with the mixture of TT and ME in different proportions (1:0, 1:0.5, 1:1, 0.5:1, 0:1).

EIS measurements confirmed that thiol composition had a direct influence on interfacial charge transfer resistance and capacitance. The 1:1 TT:ME sample exhibited the highest charge transfer resistance ($R_{CT1} = 37.62 \pm 2.51 \, k\Omega$) and the lowest double-layer capacitance, indicating a dense and defect-minimized monolayer that acted as an effective dielectric barrier. I interpreted these results as evidence that the TT:ME combination produced optimal molecular packing, where TT provided strong S–Au anchoring and ME filled the interstitial spaces, reducing pinholes and minimizing electrolyte penetration to the underlying Au surface. This dense packing likely suppressed electron tunneling pathways, leading to the highest insulating performance among the tested ratios.

In contrast, ME-rich SAMs (0:1) exhibited a significantly higher CSC (21.9 ± 1.0 mC cm⁻²) and lower R_{CT}. I attributed this to partial oxidation of ME at positive potentials, producing redox-active sites that contributed to pseudocapacitance in addition to double-layer charging. Bare Au, by comparison, had a CSC of 10.4 ± 0.8 mC cm⁻² and low R_{CT} due to its conductive, unmodified surface allowing facile electron transfer. TT-rich SAMs progressively lowered CSC values by blocking active surface sites, confirming that increased molecular order and surface coverage were associated with greater electron-transfer suppression. These electrochemical trends were consistent with my morphological observations, reinforcing the link between monolayer order, defect density, and electrochemical barrier properties.

I evaluated the cytocompatibility of thiol-based SAM coatings using a primary mixed neural culture derived from the embryonic ventral mesencephalon, grown on both unmodified Au controls and TT:ME-modified surfaces for up to 10 days in vitro. Representative fluorescence images (Figure 12 (A)) showed neurons (red), astrocytes (green), and nuclei (blue). On the Au control, the cellular composition after 10 days consisted of approximately 22% astrocytes and 78% neurons (Figure 12 (B)), which I used as a baseline for comparison. All thiol-modified samples with TT:ME ratios of 1:0.5, 1:1, and 0:1 showed reduced astrocyte percentages below 18%, with the lowest value of 10% observed for the 0.5:1 formulation. This trend indicated that altering the surface composition modestly promoted neuronal viability while suppressing astrocytic proliferation compared to bare Au.

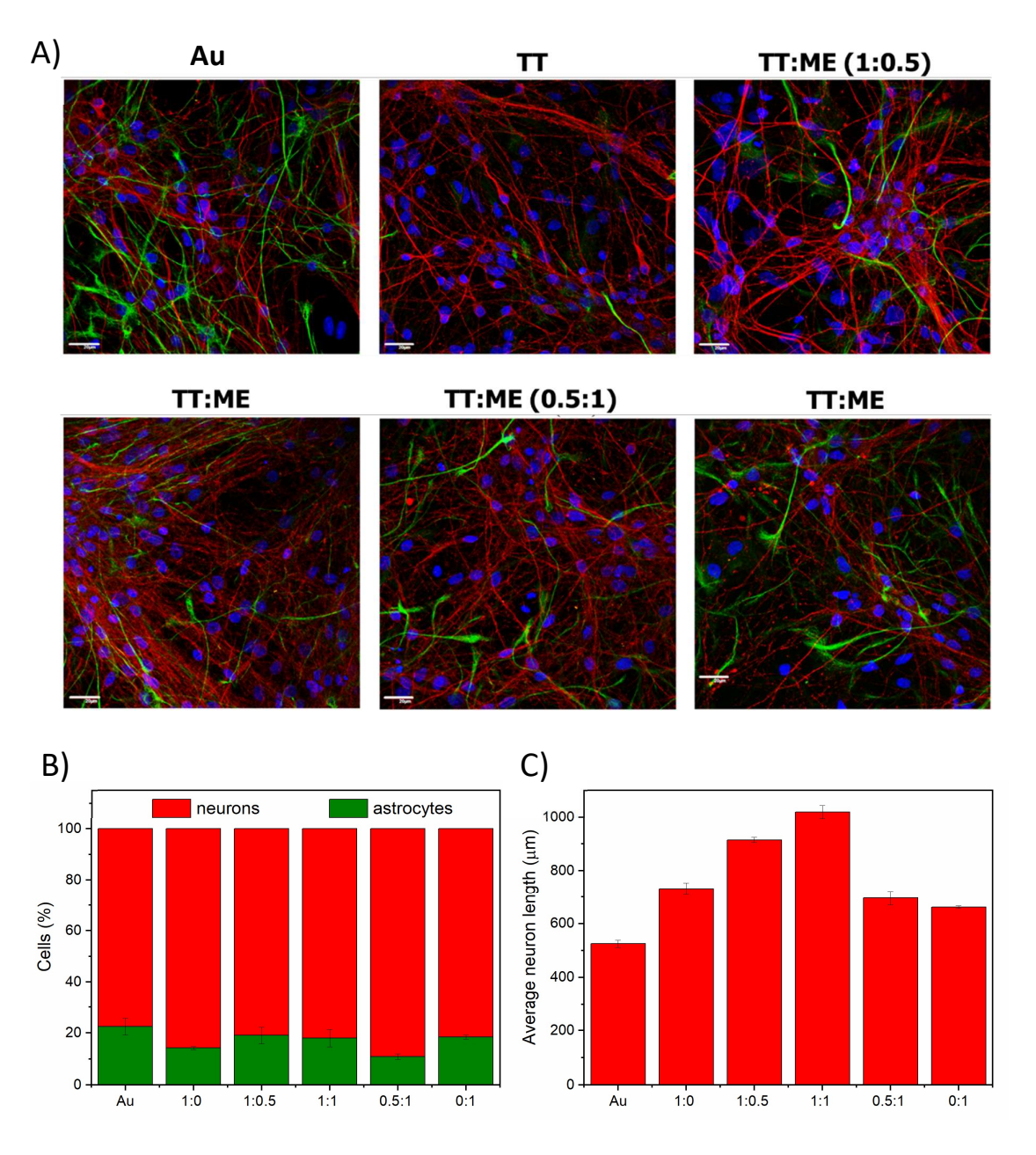


Figure 12 - Fluorescent images of primary ventral mesencephalic mixed cell population cultured on an unmodified Au surface as well as Au surfaces modified with the mixture of TT and ME in different proportions for 10 days (A); neurons are visualized by anti- β III tubulin (red), astrocyte cells by anti-GFAP (green) and nuclei by DAPI (blue), scale bar = 20 μ m. Cell density (%) of astrocytes and neurons (B); average neurite length, μ m (C); results are expressed as the mean \pm standard error of the mean.

Neurite outgrowth analysis (Figure 12 (C)) revealed that the unmodified Au surface, with its relatively high roughness, supported only moderate neurite extension ($525 \pm 13 \mu m$), likely due to disrupted cell adhesion caused by its coarse and heterogeneous topography⁶⁷. Thiol modification enhanced neurite outgrowth across all formulations, with the extent depending on the TT:ME ratio. The TT-only coating (1:0) yielded modest improvement ($732 \pm 22 \mu m$), reflecting reduced roughness but limited chemical diversity. Progressive incorporation of ME decreased surface roughness and further improved neurite extension, with the 1:1 ratio producing the longest neurites ($1018 \pm 24 \mu m$), suggesting that a balanced mix of hydrophobic TT and hydrophilic ME created an optimal microenvironment for protein adsorption and neuronal adhesion¹³. However, higher ME content in 0.5:1 and 0:1 formulations slightly reduced neurite length ($696 \pm 25 \mu m$ and $661 \pm 5 \mu m$, respectively).

I further evaluated neuronal cytocompatibility on functionalized gold substrates by analyzing the fractal dimension (FD) to assess how thiol-based SAMs influenced cell growth. Neurons with high FD values (Figure 13 (A)) exhibited extensive branching and connectivity, whereas elevated FD values in astrocytes (Figure 13 (B)) suggested increased reactivity, potentially associated with glial scarring⁶⁸. On unmodified Au surfaces, neurons displayed an FD of 1.79 \pm 0.01, indicating moderate dendritic branching, while astrocytes showed a higher FD of 1.57 ± 0.01 , consistent with notable activation and possible proinflammatory signaling. The TT-only surface (1:0) maintained a similar neuronal FD (1.77 \pm 0.01) but reduced astrocytic branching complexity to 1.37 ± 0.07 , suggesting suppressed astrocyte activation. The 1:0.5 formulation slightly lowered neuronal FD to 1.69 ± 0.02 while maintaining low astrocytic FD (1.45 ± 0.03) , supporting neuronal growth while limiting glial reactivity. The 1:1 ratio proved particularly favorable, producing the highest neuronal FD (1.84 \pm 0.02), indicative of enhanced dendritic complexity, alongside a moderately low astrocytic FD (1.52 \pm 0.02), suggesting a balanced glial response that supports neuronal network formation. In contrast, the ME-only coating (0:1) yielded the lowest neuronal FD (1.66 ± 0.01) and reduced astrocytic complexity (1.47 ± 0.01) , indicating minimal support for neurite branching and limited neuronal network development.

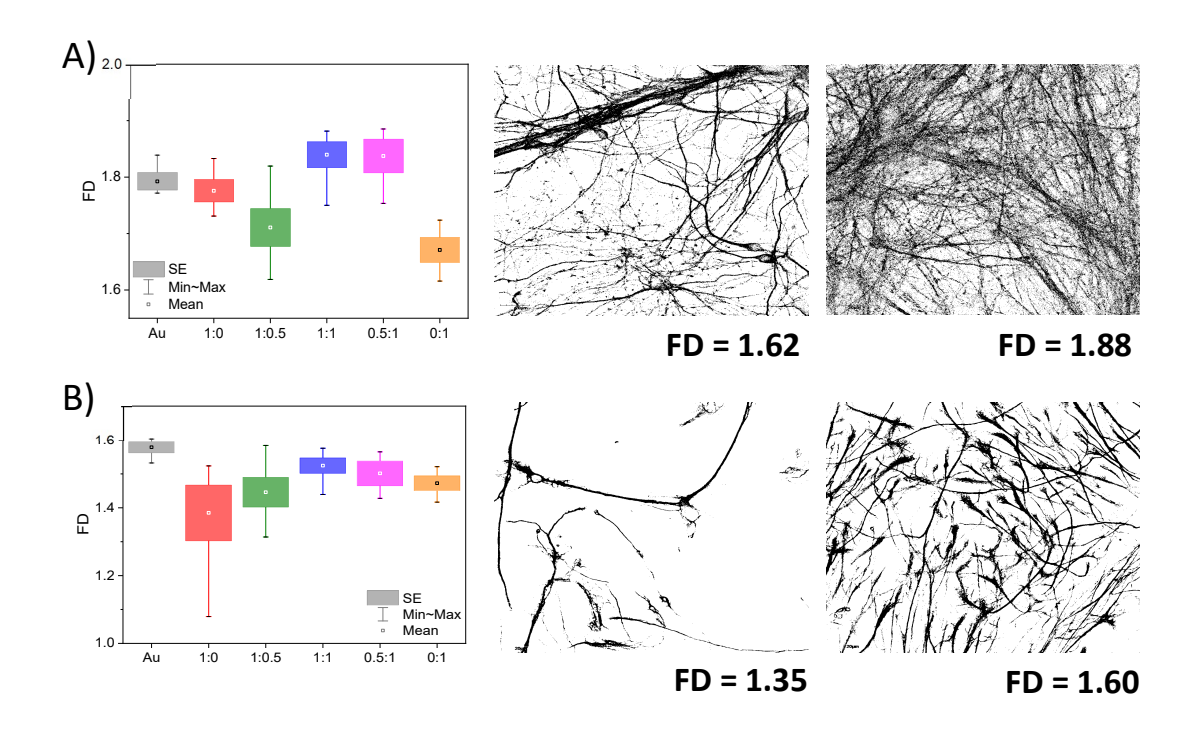


Figure 13 - Fractal dimension of neurons (A) and astrocytes (B) cultured on the surface of an unmodified Au surface as well as Au surfaces modified with the mixture of TT and ME in different proportions for 10 days, with the examples of binary images for both neurons and astrocytes characterized by lowest and highest fractal dimensions.

This chapter demonstrates that the interfacial properties of gold neural electrodes can be precisely tuned using binary self-assembled monolayers of structurally distinct thiols. By combining the hydrophobic, π -conjugated character of 2-thiophenethiol with the hydrophilic, hydroxyl-rich structure of 2-mercaptoethanol, I engineered surfaces that simultaneously optimized electrochemical stability and selective biological compatibility. The 1:1 TT:ME layer emerged as a high-performance biointerface, offering a favourable balance of surface roughness, impedance, and charge storage capacity, while dramatically enhancing neurite outgrowth and minimizing astrocytic activation. These findings establish that subtle modulation of thiol composition at the molecular level can direct complex multicellular responses providing an elegant, scalable strategy for tailoring bioelectrode interfaces without requiring polymer films or external patterning. This work advances the fundamental understanding of SAM-mediated neural integration and offers a blueprint for designing next-generation electrode coatings that combine electrochemical precision with targeted biological outcomes.

5. Summary

This dissertation investigates ultrathin, molecularly engineered organic coatings as a route to reconcile electrical performance with biological integration at metal electrodes used in implantable biomedical devices. The work opens with a critical synthesis of the literature on electrode materials and surface engineering, establishing why monolayer-scale strategies are attractive: noble-metal electrodes remain indispensable for stability and conductivity, yet at small feature sizes they suffer from high interfacial impedance, while their rigid and chemically inert surfaces can trigger adverse tissue responses that degrade function over time. Bulk overcoats such as conducting polymers and hydrogels can temporarily lower impedance or soften mechanics, but they often sacrifice long-term adhesion, chemical stability, or molecular control of biointeractions. This landscape motivates a shift toward coatings that preserve the conduction pathways of the metal while programming the interface chemistry with nanometer precision.

Against this backdrop, the thesis formulates and tests the hypothesis that covalently grafted aryl layers formed by diazonium or iodonium electrografting and self-assembled thiol monolayers can be composed to stabilize charge transfer, steer neuron-glia interactions, and incorporate contact-active antimicrobial protection. A shared methodology underpins all studies: cyclic voltammetry and electrochemical impedance spectroscopy to quantify interfacial charge transport and capacitive behavior; AFM, profilometry and wettability to resolve morphology and surface energy; and quantitative biological assays to evaluate neuronal adhesion and differentiation and astrocytic behavior. This toolbox enables structure function mapping from molecular design to device-level metrics.

The first chapter establishes diazonium electrografting as a robust covalent scaffold for neural biofunctionality. Aryl layers formed on platinum support stable presentation of poly-L-lysine and laminin; while physical adsorption improves adhesion only modestly, amide coupling via EDC produces dense, persistent peptide interfaces that enhance neuronal attachment and differentiation markers and suppress glial motility. These results demonstrate that anchoring chemistry and ECM-mimetic cues can be combined to bias cell-type outcomes at the interface while resisting wash-off properties essential for chronic devices.

A second thread addresses a long-standing barrier in polymer-based electrodes: delamination of PEDOT:PSS from metallic substrates. Electrografted iodonium interlayers provide reproducible, mild-processing adhesion promotion that strengthens polymer cohesion without

compromising electrochemical performance. After PEDOT deposition, the modified electrodes retain low impedance and high charge-storage capacity and withstand electrochemical operation with reduced mechanical damage, directly improving the reliability of conducting-polymer coatings under realistic stresses.

To probe fine chemical control of neural responses without thick films, the thesis then examines mixed self-assembled monolayers on gold, blending 2-thiophenethiol and 2-mercaptoethanol to tune wettability, packing, and interfacial impedance. Composition-dependent electrochemical signatures correlate with biological outcomes: intermediate compositions support neurite outgrowth while limiting astrocytic branching complexity. These findings position SAM blending as a practical design handle for cell-type-aware interfaces that remain electrically efficient.

Taken together, the results support a modular strategy for engineering metal—tissue interfaces with molecular precision. Covalent aryl grafting supplies durable foundations for bioactive ligands and conducting polymers; mixed thiol monolayers provide granular control of interfacial charge and wettability linked to neuron-favoring along with astrocyte-moderating responses. By moving from bulk films to programmed monolayers, the thesis shows that it is possible to simultaneously enhance electrical stability, and shape cellular behavior, key prerequisites for reliable, multifunctional implantable biosensors and neural interfaces. The concluding perspective outlines design guidelines and immediate next steps, including chronic stability studies in relevant environments, integration with microfabricated arrays, and translation of the monolayer toolkit to additional device classes where long-term electrochemical performance and biological integration must coexist.

References

- (1) Li, J.; Zhang, W.; Liao, Y.; Qiu, Y.; Zhu, Y.; Zhang, X.; Wang, C. Neural Decoding Reliability: Breakthroughs and Potential of Brain—Computer Interfaces Technologies in the Treatment of Neurological Diseases. *Phys. Life Rev.* **2025**, *55* (August), 1–40. https://doi.org/10.1016/j.plrev.2025.08.007.
- (2) Lv, S.; Xu, Z.; Mo, F.; Wang, Y.; Duan, Y.; Liu, Y.; Jing, L.; Shan, J.; Jia, Q.; Wang, M.; Zhang, S.; Liu, Y.; Liu, J.; Luo, J.; Wu, Y.; Wang, M.; Song, Y.; Cai, X. Long-Term Stability Strategies of Deep Brain Flexible Neural Interface. *npj Flex. Electron.* **2025**, *9* (1), 40. https://doi.org/10.1038/s41528-025-00410-x.
- (3) Redolfi Riva, E.; Micera, S. Progress and Challenges of Implantable Neural Interfaces Based on Nature-Derived Materials. *Bioelectron. Med.* **2021**, *7* (1), 6. https://doi.org/10.1186/s42234-021-00067-7.
- (4) Patel, T.; Huang, J.; Krukiewicz, K. Multifunctional Organic Monolayer-Based Coatings for Implantable Biosensors and Bioelectronic Devices: Review and Perspectives. *Biosens. Bioelectron. X* **2023**, *14* (December 2022), 100349. https://doi.org/10.1016/j.biosx.2023.100349.
- (5) Lee, S. H.; Yoo, S.; Kim, S. H.; Kim, Y. M.; Han, S. I.; Lee, H. Nature-Inspired Surface Modification Strategies for Implantable Devices. *Mater. Today Bio* **2025**, *31* (February), 101615. https://doi.org/10.1016/j.mtbio.2025.101615.
- (6) Gori, M.; Vadalà, G.; Giannitelli, S. M.; Denaro, V.; Di Pino, G. Biomedical and Tissue Engineering Strategies to Control Foreign Body Reaction to Invasive Neural Electrodes. *Front. Bioeng. Biotechnol.* **2021**, *9* (May), 1–26. https://doi.org/10.3389/fbioe.2021.659033.
- (7) Maiolo, L.; Guarino, V.; Saracino, E.; Convertino, A.; Melucci, M.; Muccini, M.; Ambrosio, L.; Zamboni, R.; Benfenati, V. Glial Interfaces: Advanced Materials and Devices to Uncover the Role of Astroglial Cells in Brain Function and Dysfunction. *Adv. Healthc. Mater.* **2021**, *10* (1), 1–28. https://doi.org/10.1002/adhm.202001268.
- (8) Yao, B.; Scalco de Vasconcelos, L.; Cui, Q.; Cardenas, A.; Yan, Y.; Du, Y.; Wu, D.; Wu, S.; Hsiai, T. K.; Lu, N.; Zhu, X.; He, X. High-Stability Conducting Polymer-Based Conformal Electrodes for Bio-/Iono-Electronics. *Mater. Today* **2022**, *53* (March), 84–97. https://doi.org/10.1016/j.mattod.2021.12.002.
- (9) Lu, P.; Ruan, D.; Huang, M.; Tian, M.; Zhu, K.; Gan, Z.; Xiao, Z. Harnessing the Potential of Hydrogels for Advanced Therapeutic Applications: Current Achievements and Future Directions. *Signal Transduct. Target. Ther.* **2024**, *9* (1). https://doi.org/10.1038/s41392-024-01852-x.
- (10) Simon, P.; Burke, A. Nanostructured Carbons: Double-Layer Capacitance and More. *Electrochem. Soc. Interface* **2008**, *17* (1), 38–43. https://doi.org/10.1149/2.F05081IF.
- (11) Mévellec, V.; Roussel, S.; Tessier, L.; Chancolon, J.; Mayne-L'Hermite, M.; Deniau, G.; Viel, P.; Palacin, S. Grafting Polymers on Surfaces: A New Powerful and Versatile Diazonium Salt-Based One-Step Process in Aqueous Media. *Chem. Mater.* 2007, 19 (25), 6323–6330. https://doi.org/10.1021/cm071371i.
- (12) Pinson, J.; Podvorica, F. I. Surface Modification of Materials: Electrografting of Organic Films. *Curr. Opin. Electrochem.* **2020**, *24* (v), 44–48.

- https://doi.org/10.1016/j.coelec.2020.05.016.
- (13) Vericat, C.; Vela, M. E.; Benitez, G.; Carro, P.; Salvarezza, R. C. Self-Assembled Monolayers of Thiols and Dithiols on Gold: New Challenges for a Well-Known System. *Chem. Soc. Rev.* **2010**, *39* (5), 1805–1834. https://doi.org/10.1039/b907301a.
- (14) Hetemi, D.; Noël, V.; Pinson, J. Grafting of Diazonium Salts on Surfaces: Application to Biosensors. *Biosensors* **2020**, *10* (1), 4. https://doi.org/10.3390/bios10010004.
- (15) Flynn, N. T.; Tran, T. N. T.; Cima, M. J.; Langer, R. Long-Term Stability of Self-Assembled Monolayers in Biological Media. *Langmuir* **2003**, *19* (26), 10909–10915. https://doi.org/10.1021/la035331e.
- (16) Bondarenko, A. S.; Ragoisha, G. A. EIS Spectrum Analyser. *Prog. Chemom. Res.* **2005**, 88–102.
- (17) Mahouche-Chergui, S.; Gam-Derouich, S.; Mangeney, C.; Chehimi, M. M. Aryl Diazonium Salts: A New Class of Coupling Agents for Bonding Polymers, Biomacromolecules and Nanoparticles to Surfaces. *Chem. Soc. Rev.* 2011, 40 (7), 4143–4166. https://doi.org/10.1039/c0cs00179a.
- (18) Pinson, J.; Podvorica, F. Attachment of Organic Layers to Conductive or Semiconductive Surfaces by Reduction of Diazonium Salts. *Chem. Soc. Rev.* **2005**, *34* (5), 429–439. https://doi.org/10.1039/b406228k.
- (19) Bélanger, D.; Pinson, J. Electrografting: A Powerful Method for Surface Modification. *Chem. Soc. Rev.* **2011**, *40* (7), 3995–4048. https://doi.org/10.1039/c0cs00149j.
- (20) Samanta, S.; Gaad, D.; Cabet, E.; Lilienbaum, A.; Singh, A.; Aswal, D. K.; Chehimi, M. M. Flexible, Biocompatible PET Sheets: A Platform for Attachment, Proliferation and Differentiation of Eukaryotic Cells. *Surfaces* 2021, 4 (4), 306–322. https://doi.org/10.3390/surfaces4040026.
- (21) Zheng, M.; Pan, M.; Zhang, W.; Lin, H.; Wu, S.; Lu, C.; Tang, S.; Liu, D.; Cai, J. Poly(α-L-Lysine)-Based Nanomaterials for Versatile Biomedical Applications: Current Advances and Perspectives. *Bioact. Mater.* 2021, 6 (7), 1878–1909. https://doi.org/10.1016/j.bioactmat.2020.12.001.
- (22) Green, R. A.; Lovell, N. H.; Wallace, G. G.; Poole-Warren, L. A. Conducting Polymers for Neural Interfaces: Challenges in Developing an Effective Long-Term Implant. *Biomaterials* **2008**, *29* (24–25), 3393–3399. https://doi.org/10.1016/j.biomaterials.2008.04.047.
- (23) Cho, Y. W.; Park, S. A.; Han, T. H.; Son, D. H.; Park, J. S.; Oh, S. J.; Moon, D. H.; Cho, K. J.; Ahn, C. H.; Byun, Y.; Kim, I. S.; Kwon, I. C.; Kim, S. Y. In Vivo Tumor Targeting and Radionuclide Imaging with Self-Assembled Nanoparticles: Mechanisms, Key Factors, and Their Implications. *Biomaterials* **2007**, *28* (6), 1236–1247. https://doi.org/10.1016/j.biomaterials.2006.10.002.
- (24) Daems, N.; Wouters, J.; Van Goethem, C.; Baert, K.; Poleunis, C.; Delcorte, A.; Hubin, A.; Vankelecom, I. F. J.; Pescarmona, P. P. Selective Reduction of Nitrobenzene to Aniline over Electrocatalysts Based on Nitrogen-Doped Carbons Containing Non-Noble Metals. *Appl. Catal. B Environ.* 2018, 226 (January), 509–522. https://doi.org/10.1016/j.apcatb.2017.12.079.
- (25) Ranella, A.; Barberoglou, M.; Bakogianni, S.; Fotakis, C.; Stratakis, E. Tuning Cell

- Adhesion by Controlling the Roughness and Wettability of 3D Micro/Nano Silicon Structures. *Acta Biomater.* **2010**, *6* (7), 2711–2720. https://doi.org/10.1016/j.actbio.2010.01.016.
- (26) Luo, J.; Walker, M.; Xiao, Y.; Donnelly, H.; Dalby, M. J.; Salmeron-Sanchez, M. The Influence of Nanotopography on Cell Behaviour through Interactions with the Extracellular Matrix A Review. *Bioact. Mater.* **2022**, *15* (August 2021), 145–159. https://doi.org/10.1016/j.bioactmat.2021.11.024.
- (27) Patel, T.; Skorupa, M.; Skonieczna, M.; Turczyn, R.; Krukiewicz, K. Surface Grafting of Poly-L-Lysine via Diazonium Chemistry to Enhance Cell Adhesion to Biomedical Electrodes. *Bioelectrochemistry* **2023**, *152* (October 2022). https://doi.org/10.1016/j.bioelechem.2023.108465.
- (28) Zhu, H.; Liu, R.; Shang, Y.; Sun, L. Polylysine Complexes and Their Biomedical Applications. *Eng. Regen.* **2023**, *4* (1), 20–27. https://doi.org/10.1016/j.engreg.2022.11.001.
- (29) Sharma, S.; Naldrett, M. J.; Gill, M. J.; Checco, J. W. Affinity-Driven Aryl Diazonium Labeling of Peptide Receptors on Living Cells. *J. Am. Chem. Soc.* **2024**, *146* (19), 13676–13688. https://doi.org/10.1021/jacs.4c04672.
- (30) Rogers, R. S.; Nishimune, H. The Role of Laminins in the Organization and Function of Neuromuscular Junctions. *Matrix Biol.* **2017**, *57–58*, 86–105. https://doi.org/10.1016/j.matbio.2016.08.008.
- (31) Nirwane, A.; Yao, Y. Laminins and Their Receptors in the CNS. *Biol. Rev.* **2019**, *94*, 283–306. https://doi.org/10.1111/brv.12454.
- (32) Torre-ubieta, L. De; Bonni, A. Review Transcriptional Regulation of Neuronal Polarity and Morphogenesis in the Mammalian Brain. *Neuron* **2011**, *72* (1), 22–40. https://doi.org/10.1016/j.neuron.2011.09.018.
- (33) Hakanen, J.; Ruiz-reig, N.; Tissir, F.; Francis, F. Linking Cell Polarity to Cortical Development and Malformations. *Front. Cell. Neurosci.* **2019**, *13* (244), 1–22. https://doi.org/10.3389/fncel.2019.00244.
- (34) Kim, Y. H.; Baek, N. S.; Han, Y. H.; Chung, M. A.; Jung, S. D. Enhancement of Neuronal Cell Adhesion by Covalent Binding of Poly-d-Lysine. *J. Neurosci. Methods* **2011**, *202* (1), 38–44. https://doi.org/10.1016/j.jneumeth.2011.08.036.
- (35) Papadimitriou, L.; Manganas, P.; Ranella, A.; Stratakis, E. Biofabrication for Neural Tissue Engineering Applications. *Mater. Today Bio* **2020**, *6* (January), 100043. https://doi.org/10.1016/j.mtbio.2020.100043.
- (36) Reuter, M.; Schwieger, C.; Meister, A.; Karlsson, G.; Blume, A. Poly-l-Lysines and Poly-l-Arginines Induce Leakage of Negatively Charged Phospholipid Vesicles and Translocate through the Lipid Bilayer upon Electrostatic Binding to the Membrane. *Biophys. Chem.* **2009**, *144* (1–2), 27–37. https://doi.org/10.1016/j.bpc.2009.06.002.
- (37) Arimori, T.; Miyazaki, N.; Mihara, E.; Takizawa, M.; Taniguchi, Y.; Cabañas, C.; Sekiguchi, K.; Takagi, J. Structural Mechanism of Laminin Recognition by Integrin. *Nat. Commun.* **2021**, *12* (1), 1–13. https://doi.org/10.1038/s41467-021-24184-8.
- (38) Chen, C.; Kong, X.; Lee, I. S. Modification of Surface/Neuron Interfaces for Neural Cell-Type Specific Responses: A Review. *Biomed. Mater.* **2015**, *11* (1).

- https://doi.org/10.1088/1748-6041/11/1/014108.
- (39) Seiti, M.; Giuri, A.; Esposito, C.; Ferraris, E. Biomaterials Advances Advancements in Tailoring PEDOT: PSS Properties for Bioelectronic Applications: A Comprehensive Review. *Biomater. Adv.* **2023**, *154*, 213655. https://doi.org/10.1016/j.bioadv.2023.213655.
- (40) Mantione, D.; Agua, I.; Sanchez-sanchez, A.; Mecerreyes, D. Poly(3,4-Ethylenedioxythiophene) (PEDOT) Derivatives: Innovative Conductive Polymers for Bioelectronics. *Polymers (Basel)*. **2017**, *9* (8), 354. https://doi.org/10.3390/polym9080354.
- (41) Liu, H.; Song, J.; Zhao, Z.; Zhao, S.; Tian, Z.; Yan, F. Organic Electrochemical Transistors for Biomarker Detections. *Adv. Sci.* **2024**, *11* (27), 1–30. https://doi.org/10.1002/advs.202305347.
- (42) Song, J.; Liu, H.; Zhao, Z.; Lin, P.; Yan, F. Flexible Organic Transistors for Biosensing: Devices and Applications. *Adv. Mater.* **2024**, *36* (20), 1–49. https://doi.org/10.1002/adma.202300034.
- (43) Donahue, M. J.; Sanchez-sanchez, A.; Inal, S.; Qu, J.; Mecerreyes, D.; Malliaras, G. G.; Martin, D. C.; Owens, R. M. Materials Science & Engineering R Tailoring PEDOT Properties for Applications in Bioelectronics. *Mater. Sci. Eng. R* 2020, 140, 100546. https://doi.org/10.1016/j.mser.2020.100546.
- (44) Smołka, S.; Skorupa, M.; Barylski, A.; Basiaga, M.; Krukiewicz, K. Electrochemistry Communications Improved Adhesion and Charge Transfer between PEDOT: PSS and the Surface of a Platinum Electrode through a Diazonium Chemistry Route Pobrano z / Downloaded from Repository of University of Silesia 2025-08-11 14: 18. *Electrochem. commun.* 2023, 153, 107528. https://doi.org/10.1016/j.elecom.2023.107528.
- (45) Haensch, C.; Schubert, U. S.; Hoeppener, S. Chemical Modification of Self-Assembled Silane Based Monolayers by Surface Reactions. *Chem. Soc. Rev.* **2010**, *39*, 2323–2334. https://doi.org/10.1039/b920491a.
- (46) Patel, T.; Skonieczna, M.; Turczyn, R.; Krukiewicz, K. Modulating Pro-Adhesive Nature of Metallic Surfaces through a Polypeptide Coupling via Diazonium Chemistry. *Sci. Rep.* **2023**, *13* (1). https://doi.org/10.1038/s41598-023-45694-z.
- (47) Koefoed, L.; Pedersen, S. Us.; Daasbjerg, K. Grafting of Aryl Diazonium, Iodonium, and Sulfonium Salts in Unusual Patterns by Exploiting the Potential Gradient in Bipolar Electrochemistry. *ChemElectroChem* **2016**, *3* (3), 495–501. https://doi.org/10.1002/celc.201500512.
- (48) Xie, X. Q.; Zhou, W.; Yang, R.; Song, X. R.; Luo, M. J.; Xiao, Q. Electroreduction Strategy: A Sustainable Tool for the Generation of Aryl Radicals. *Org. Chem. Front.* **2024**, *11* (15), 4318–4342. https://doi.org/10.1039/d4qo00846d.
- (49) Muñiz, K. Promoting Intermolecular C-N Bond Formation under the Auspices of Iodine(III). *Acc. Chem. Res.* **2018**, *51* (6), 1507–1519. https://doi.org/10.1021/acs.accounts.8b00137.
- (50) Steeno, R.; Rodríguez González, M. C.; Eyley, S.; Thielemans, W.; Mali, K. S.; De Feyter, S. Covalent Functionalization of Carbon Surfaces: Diaryliodonium versus

- Aryldiazonium Chemistry. *Chem. Mater.* **2020**, *32* (12), 5246–5255. https://doi.org/10.1021/acs.chemmater.0c01393.
- (51) Combellas, C.; Jiang, D. E.; Kanoufi, F.; Pinson, J.; Podvorica, F. I. Steric Effects in the Reaction of Aryl Radicals on Surfaces. *Langmuir* **2009**, *25* (1), 286–293. https://doi.org/10.1021/la8025792.
- (52) Miliutina, E.; Guselnikova, O.; Soldatova, N. S.; Bainova, P.; Elashnikov, R.; Fitl, P.; Kurten, T.; Yusubov, M. S.; Švorčík, V.; Valiev, R. R.; Chehimi, M. M.; Lyutakov, O.; Postnikov, P. S. Can Plasmon Change Reaction Path? Decomposition of Unsymmetrical Iodonium Salts as an Organic Probe. *J. Phys. Chem. Lett.* 2020, 11 (14), 5770–5776. https://doi.org/10.1021/acs.jpclett.0c01350.
- (53) Li, F.; Meng, R.; Wang, W.; Wang, W.; Jin, B. Effect of Electron-Donating Groups on the Electrochemical Degradation of Aromatic Nitro Compounds in Aprotic Media Containing CO2. *J. Phys. Chem. C* **2021**, *125* (30), 16464–16472. https://doi.org/10.1021/acs.jpcc.1c01413.
- (54) Koefoed, L.; Vase, K. H.; Stenlid, J. H.; Brinck, T.; Yoshimura, Y.; Lund, H.; Pedersen, S. U.; Daasbjerg, K. On the Kinetic and Thermodynamic Properties of Aryl Radicals Using Electrochemical and Theoretical Approaches. *ChemElectroChem* 2017, 4 (12), 3212–3221. https://doi.org/10.1002/celc.201700772.
- (55) Feng, Q. K.; Zhong, S. L.; Pei, J. Y.; Zhao, Y.; Zhang, D. L.; Liu, D. F.; Zhang, Y. X.; Dang, Z. M. Recent Progress and Future Prospects on All-Organic Polymer Dielectrics for Energy Storage Capacitors. *Chem. Rev.* **2022**, *122* (3), 3820–3878. https://doi.org/10.1021/acs.chemrev.1c00793.
- (56) Li, W.; Li, Y.; Song, Z.; Wang, Y. X.; Hu, W. PEDOT-Based Stretchable Optoelectronic Materials and Devices for Bioelectronic Interfaces. *Chem. Soc. Rev.* **2024**, *53* (21), 10575–10603. https://doi.org/10.1039/d4cs00541d.
- (57) Gao, X.; Bao, Y.; Chen, Z.; Lu, J.; Su, T.; Zhang, L.; Ouyang, J. Bioelectronic Applications of Intrinsically Conductive Polymers. *Adv. Electron. Mater.* **2023**, *9* (10), 1–26. https://doi.org/10.1002/aelm.202300082.
- (58) Smołka, S.; Patel, T.; Pluczyk-Małek, S.; Turczyn, R.; Krukiewicz, K. Iodonium-Based pro-Adhesive Layers for Robust Adhesion of PEDOT:PSS to Surfaces. *Sci. Technol. Adv. Mater.* **2024**, *25* (1). https://doi.org/10.1080/14686996.2024.2338786.
- (59) Lee, I.; Park, S.; Lee, Y. S.; Kim, Y.; Kang, M. H.; Yun, C. Gradual Morphological Change in PEDOT:PSS Thin Films Immersed in an Aqueous Solution. *Langmuir* **2023**, *39* (4), 1600–1610. https://doi.org/10.1021/acs.langmuir.2c03038.
- (60) Kim, S. M.; Kim, C. H.; Kim, Y.; Kim, N.; Lee, W. J.; Lee, E. H.; Kim, D.; Park, S.; Lee, K.; Rivnay, J.; Yoon, M. H. Influence of PEDOT:PSS Crystallinity and Composition on Electrochemical Transistor Performance and Long-Term Stability. *Nat. Commun.* 2018, 9 (1). https://doi.org/10.1038/s41467-018-06084-6.
- (61) Tanwar, A. S.; Meyer, F. Harnessing Non-Covalent Interactions in Modified Thiophenes: Structural Design and Applications in Materials and Biological Sciences. *CrystEngComm* **2025**, *27* (6), 736–748. https://doi.org/10.1039/d4ce01213e.
- (62) Zukauskas, S.; Rucinskiene, A.; Ratautaite, V.; Ramanaviciene, A.; Pilvenyte, G.; Bechelany, M.; Ramanavicius, A. Electrochemical Biosensor for the Determination of

- Specific Antibodies against SARS-CoV-2 Spike Protein. *Int. J. Mol. Sci.* **2023**, *24* (1). https://doi.org/10.3390/ijms24010718.
- (63) Weisshaar, D. E.; Walczak, M. M.; Porter, M. D. Electrochemically Induced Transformations of Monolayers Formed by Self-Assembly of Mercaptoethanol at Gold. *Langmuir* **1993**, *9* (1), 323–329. https://doi.org/10.1021/la00025a061.
- (64) Love, J. C.; Estroff, L. A.; Kriebel, J. K.; Nuzzo, R. G.; Whitesides, G. M. Self-Assembled Monolayers of Thiolates on Metals as a Form of Nanotechnology. *Chem. Rev.* **2005**, *105* (4), 1103–1169. https://doi.org/10.1021/cr0300789.
- (65) Borzenkov, M.; Chirico, G.; D'Alfonso, L.; Sironi, L.; Collini, M.; Cabrini, E.; Dacarro, G.; Milanese, C.; Pallavicini, P.; Taglietti, A.; Bernhard, C.; Denat, F. Thermal and Chemical Stability of Thiol Bonding on Gold Nanostars. *Langmuir* **2015**, *31* (29), 8081–8091. https://doi.org/10.1021/acs.langmuir.5b01473.
- (66) Biswal, H. S.; Shirhatti, P. R.; Wategaonkar, S. O-H···O versus O-H···S Hydrogen Bonding. 2. Alcohols and Thiols as Hydrogen Bond Acceptors. *J. Phys. Chem. A* **2010**, 114 (26), 6944–6955. https://doi.org/10.1021/jp102346n.
- (67) Dastjerdi, A. K.; Pagano, M.; Kaartinen, M. T.; McKee, M. D.; Barthelat, F. Cohesive Behavior of Soft Biological Adhesives: Experiments and Modeling. *Acta Biomater*. **2012**, *8* (9), 3349–3359. https://doi.org/10.1016/j.actbio.2012.05.005.
- (68) Sołtys, Z.; Ziaja, M.; Pawliński, R.; Setkowicz, Z.; Janeczko, K. Morphology of Reactive Microglia in the Cerebral Cortex. Fractal Analysis and Complementary Quantitative Methods. *J. Neurosci. Res.* **2001**, *63* (1), 90–97. https://doi.org/10.1002/1097-4547(20010101)63:1<90::AID-JNR11>3.0.CO;2-9.

Summary of personal contribution

[R1] Contribution: Conceived and structured the outline of the review. Conducted an extensive literature survey, critically analysing over 200 sources related to organic monolayer-based coatings, electrografting techniques, and their applications in implantable biosensors and bioelectronic devices. Synthesized information across multidisciplinary fields (surface chemistry, material science, biointerfaces, and clinical applications) and wrote the majority of the manuscript including the introduction, biomaterial sections (noble metals, carbonaceous materials, soft/elastic polymers, biodegradable electrodes), diazonium/iodonium/sulfonium sections, and the discussion on challenges (biocompatibility, biofouling, bacterial colonization, long-term stability). Coordinated figure design, edited citations, managed referencing, and prepared the manuscript for submission.

My overall contribution to this research was equal to 70%.

[R2] Contribution: Led the project execution and manuscript preparation. Primarily responsible for optimizing the diazonium-based surface grafting protocol, preparing and modifying electrode samples, and conducting electrogravimetric (EQCM) and electrochemical (CV, EIS) analyses. Performed comprehensive surface characterization (including profilometry, contact angle measurements, and FTIR spectroscopy), evaluated physicochemical surface properties post-grafting, and conducted all data processing and visualization (graphs, statistical analysis). Wrote the initial draft of the manuscript.

My overall contribution to this research was equal to 60%.

[R3] Contribution: Conceived and executed the majority of the experimental work. Synthesized diazonium salts, optimized electrografting conditions for coupling poly-L-lysine to metallic substrates and performed detailed electrochemical characterization using cyclic voltammetry and electrochemical impedance spectroscopy. Conducted surface analysis including contact angle measurements and profilometry, processed and interpreted data on adhesion and morphological changes across various metallic surfaces, and coordinated data visualization and figure generation. Wrote the initial draft of the manuscript and addressing reviewer feedback during the revision process.

My overall contribution of this research was equal to 65%.

[R4] Contribution: Co-led the study design, experimental work, and manuscript preparation. Conducted surface modification of metallic substrates with different iodonium salts and

optimized PEDOT:PSS electrodeposition. Performed electrochemical characterization (Cyclic voltammetry and Electrochemical impedance spectroscopy), adhesion assessment (tape test), and wettability evaluation (contact angle). Led figure preparation, data visualization, and coauthored the main manuscript sections including methods, results, and discussion.

My overall contribution of this research was equal to 40%.

[R5] Contribution: Performed the experimental work on thiol-based self-assembled monolayers (SAM's) for biomedical electrode coatings. Conducted electrochemical characterization (electrochemical impedance spectroscopy and cyclic voltammetry), contact angle measurements, and profilometry to evaluate surface wettability and roughness. Analysed the collected data, prepared all figures and schematic illustrations, organized the reference list, and integrated experimental results into the manuscript. Wrote the first draft of the paper, ensuring logical flow and thematic consistency.

My overall contribution to this research was equal to 40%.

List of scientific accomplishments

1. Publications and chapters other than those included in the thesis

- Synthesis and characterization of novel molybdovanadophosphoric acid supported kaolin hybrid catalyst for chromotrope 2R dye degradation in water, Patel T., Mayani VJ., Mayani SV.: SN applied sciences (Springer) 4(11), 2022, DOI: 10.1007/s42452-022-05201-x
- Development of a Sustainable Tungsten and Iron Bimetal-Immobilized SBA-15
 Composite for Enhanced Wet Catalytic Oxidation of Dye Capacity, Patel T.,
 Mayani VJ., Mayani SV.: ACS Omega 8(1), 2022, DOI:
 10.1021/acsomega.2c04549
- 3. Diazonium chemistry as a robust approach for the biofunctionalization of titanium surface, Skorupa M., **Patel T.**, Krukiewicz K.: Computational Oncology and Personalized Medicine, volume 2, 2022, DOI: 10.34918/85101.
- Bioaerosols in municipal waste as a source of microbiological pollution and health hazard, Vaishnani MJ., Mayani SV., Patel T., Deka BK.: Bioaerosols Emission from Anthropogenic Sources (Chapter 10, pg.183-198), Elsevier 2024 DOI: 10.1016/B978-0-443-15319-8.00010-1
- Surface-Functionalized PEDOT:PSS interfaces for improved adhesion, Viability, and Extracellular charge transfer of Shewanella oneidensis MR-1, Abdullah A., Shakibania S., Patel T., Shyntum DY., Krukiewicz K.; ACS Sustainable Chemistry and Engineering, 12(52), 2024, DOI: 10.1021/acssuschemeng.4c05458
- Hybrid conducting polymer films promote neural outgrowth and neuralelectrode integration in vitro; Shakibania S., Patel T., Turczyn R., Biggs M.J.P., Krukiewicz K.; Bioelectrochemistry; 2025; 165; 1-11; DOI: 10.1016/j.bioelechem.2025.108985
- Engineering conducting polymer-based interfaces for high-performance microbial electrochemical systems; Abdullah., Shyntum D.Y., Shakibania S., Patel T., Krukiewicz K.; Bioelectrochemistry; 2026; 168; 109142; DOI: 10.1016/j.bioelechem.2025.109142
- 8. Unlocking the potential of quinoline diazonium salts: An electrochemical approach for engineering antimicrobial surfaces; Patel T., Shyntum D.Y.,

Abdullah, Bogusz M., Turczyn R., Krukiewicz K.; Surfaces and Interfaces (completed first round of revision). https://dx.doi.org/10.2139/ssrn.5394209

2. Scientific conferences

- 1. Green technologies for sustainable development, Gujarat, India (In-person), 9 III-11 III 2021, Singh A., Patel T., Mayani VJ., Mayani SV.: Review on catalytic degradation of hazardous phenolic compounds using nanocatalyst@carbon (Oral Presentation).
- Recent Trends in Green Chemistry, Punjab, India in collaboration with Indian chemical society, Kolkata, India, (Online) 28 IX-30 IX 2021, Singh A., Patel T., Mayani VJ., Mayani SV.: Preparation of green and renewable gold salen nanocatalyst@carbon: catalytic degradation of hazardous pollutant dyes (Poster).
- 3. Materials of the Millennium: Emerging Trends and Future Prospects, Gujarat, India, (Online) 19 XI-21 XI, 2021, Singh A., Patel T., Mayani VJ., Mayani SV.: Synthesis of Gold@Nanocarbon composite and application in catalysis and adsorption (Poster).
- 4. Organic Bioelectronics Conference, Valencia, Spain (Online), 8 II-9 II 2022, Patel T., Krukiewicz K.: Enhancement of poly-lysine attachment to functionalized electrodes (Poster).
- 5. 10th European Young Engineers Conference, Warsaw, Poland (Online), 4 IV-6 IV 2022, **Patel T**., Krukiewicz K.: Organic monolayer-based protective coatings for bioelectronic devices (Poster).
- 6. 6th International Workshop on Nano and Bio Photonics, Evian, France (Inperson), 25 IX-30 IX 2022, Patel T., Skorupa M., Skonieczna M., Turczyn R., Krukiewicz K.: Enhancing neural cell adhesion on the surface modified with diazonium salts and poly-l-lysine (Poster).
- 7. 26th Gliwice Scientific Meetings, Gliwice, Poland (In-person), 18 XI-19 XI 2022, **Patel T.**, Skorupa M., Skonieczna M., Turczyn R., Krukiewicz K.: Surface modification via diazonium salts and poly-l-lysine to enhance neural cell adhesion (Poster).

- 8. Computational oncology and personalized medicine conference (COPM), Gliwice, Poland (In person), 26 IV 2023, Patel T, Skonieczna M, Turczyn R, Krukiewicz K: Biofunctionalization of Electrodes Enhances Cell Adhesion: A promising approach for developing functional biomaterials for neurological devices (Oral Presentation).
- 9. 37th RoMedINF Conference, Timisoara, Romania (Online), 14 IX-15 IX 2023, Skorupa M., **Patel T.,** Abdullah, Shakibania S., Shukla V., Ul Haq I., and Krukiewicz K., Development of Multifunctional Biomaterials by Combining Electrochemistry, Microbiology, and Neural Tissue Engineering (Oral presentation)
- 10. 16th International workshop on Impedance spectroscopy (IWIS), Chemnitz, Germany (In person), 26 IX- 29 IX 2023, **Patel T.**, Krukiewicz K., Exploring the Behaviour of Electrodeposited Iodonium salts: Insights from Electrochemical Impedance Spectroscopy on Coating Performance (Poster).
- 11. 75th Annual Meeting of the International Society of Electrochemistry (ISE), Montreal, Canada (In person), 18 VIII 23 VIII 2024, Patel T., Shyntum DY., Abdullah., Skorupa M., Turczyn R., Krukiewicz K., Bioelectronic Advancements: Electrodeposited Quinoline-Derived Antibacterial Coatings for Improved Biocompatibility of Implantable Neural Electrodes (Oral presentation).
- 12. American Chemical Society (ACS) fall meeting, Washington DC, United States of America (In person), 17 VIII 21 VIII 2025, **Patel T.**, Biggs M., Krukiewicz K., Self-assembled thiol monolayers as functional coatings for electrodes in stimulus-responsive neurotransmitter delivery (Oral presentation).

3. Research projects

- 03.2022-07.2023: scholarship holder in the project "Biofunctionalized organic surfaces for neuroelectronic interfaces", at the Silesian University of Technology (SUT), 2019/35/B/ST5/00995, National Science Center (NCN), within the OPUS framework.
- 2. 08.2023-12.2023: scholarship holder in a project "Multilayer electroactive coatings with hierarchical structure for controlled delivery of neurotransmitters", SUT, 2021/42/E/ST5/00165, NCN, within the SONATA-BIS framework.

4. Internship

 United States of America, Missouri University of Science and Technology, Lightwave technology laboratory, 08.2024-11.2024, under the supervision of Prof. Jie Huang.

5. Other scholarships

Rector's scholarship for the best students of the SUT coming from non-EU countries, under the excellence initiative, awarded for the 2021/2022 academic year.

Appendix